博士論文

Collective dynamics of repulsive self-propelled particles
斥力相互作用する自己駆動粒子系の集団動力学

平岡　喬之

Doctoral Thesis

COLLECTIVE DYNAMICS OF REPULSIVE SELF-PROPELLED PARTICLES

Takayuki Hiraoka

Department of Applied Physics
School of Engineering
University of Tokyo

December 2016

Acknowledgements

This dissertation marks the collection of achievements I have made in the past several years, but it would have been impossible for me to complete it on my own. Along the way, the following people have offered me generous support in terms of academic contributions as well as encouragement to my life as a graduate student.

First of all, I am thankful to my advisor Prof. Nobuyasu Ito for giving me chances and for providing a stimulating environment to pursue my study. I was lucky that I could start my academic carrier in Ito group, where the professor's open attitude and extensive knowledge have been creating a lively atmosphere. I also thank Dr. Takashi Shimada for his scientific advises as well as his guidance on how to be a productive scientist. My gratitude extends to the current and former members of the group: Dr. Naoto Aoki, Koji Oishi, Akiyuki Kuwabara, Shota Nagumo, Shuhei Miyano, and Wataru Hirotani. Among these people, extra thanks goes to Koji Oishi. I have learned a lot from communication and discussion with him.

I also feel grateful to Prof. Tamás Vicsek at Eötvös Loránd University for accepting me as a visitor to his group. The intellectual exchange with him and members of his group have broadened my perspective.

Last but not least, I would like to thank my family and my closest friends for giving me every kind of help I needed to complete my PhD course.

List of publications

- Takayuki Hiraoka, Takashi Shimada, and Nobuyasu Ito, *Collective dynamics of pedestrians with no fixed destination*, Proceedings of the Joint International Conference on Social Modeling and Simulation and Econophysics Colloquium 2014, Springer, 243 (2015)
- Takayuki Hiraoka, Takashi Shimada, and Nobuyasu Ito, *Order-disorder transition in repulsive self-propelled particle systems*, Physical Review E 94, 062612 (2016)

Contents

Chapter 1

Introduction

1.1 Ubiquity of collective motion

Among countless fascinating dynamical patterns the nature present, the most familiar one to us may be the phenomena that arise from flocking of biological objects. Most of us may have seen, either with our own eyes or in video images, a group of animals moving together: for example, birds such as pigeons, starlings, and geese fly together in the sky; farm animals such as sheep and horse and wild mammals such as zebras, buffalos, and reindeers migrate in herd; fish such as herrings and tuna swim in school; insects such as ants, termites, and mosquitos aggregate to form swarms; locusts are also known to migrate in vast swarms, which sometimes cause a severe damage to crops.

Animals are not exceptional beings in the living world that posses ability to move collectively. Some microorganisms, which inhabit typically in spatial scale of micrometers, display collective behaviors too. Motile bacteria such as *Escherichia coli* and *Bacillus subtilis* propel themselves by rotating helix-shaped flagella, and swim within colonies in a coordinated manner[1, 2]. Eukaryotic cells are also prone to collective migration. Their modes of locomotion are quite diverse: In hydrodynamic environment, a sperm cell propels itself using a flagellum at the back[3], while a *Chlamydomonas reinhardtii* swims by breaststroke-like beating of two flagella at the front[4]; on the other hand, crawling motion on a substrate, referred to as amoeboid movement, is achieved by protrusion of cellular structures called blebs and lamellipodia[5, 6]. In multicellular animals, collective cell migration plays a crucial role in embryonic development, tissue regeneration, immunity, and tumor invasion and metastasis[7, 8]. A migration mode specific to aggregated cells can be seen in a tightly adhered epithelial monolayer, which maintain their contacts with neighbors as they moves as a coherent sheet[9, 10].

Another animal that displays characteristic collective motion is *us*—the humans. Human crowds exhibit a variety of self-organized dynamic patterns in urban streets, in stadiums, in hallways, and in rooms. Several well-known phenomena from empirical findings include lane formation in bidirectional flows, oscillations of passing direction at bottlenecks, arch-like clogging around exits, and stripe formation in two intersecting streams[11, 12]. Recently, video analysis of scenes from a crowd accident revealed emergence of stop-and-go waves and crowd turbulence at high densities[13].

These far-from-exhaustive examples are already convincing enough that collective motion is abundant and ubiquitous in wide range of length scales that span from tens of micrometers up to tens of kilometers. The question for physicists is what, if at all, is the universality that dominates the various phenomena.

1.1.1 What is *flock*?

Before going any further, I would like to clarify the definition of the word *flock*. What is the *flock*, whose behavior we are trying to understand? First of all, a flock is definitely not a single individual; two or three would not be enough either. It refers to a group that consist of a number of animals moving and staying together. Reynolds[14] added a further explanation to specify the phenomena: a flock is "a group of objects that exhibits this general class of polarized, noncolliding, aggregate motion." This is a plain definition that fits well with our interest in collective motion; it also provides principles for modeling the phenomena, as we will see in the next section.

Interestingly, English is full of terms synonymous with *flock*, all being collective nouns that describe a group of animals, but each specialized to what the subject is; for example, *school* is for fish, *swarm* for insects, *herd* for hoofed mammals, *crowd* for people, etc. In Japanese, however, they are all described in a single word "*mure*."

1.2 Mathematical modeling

1.2.1 Reynolds boid model

The first attempts at constructing a mathematical model that reproduce the flocking behavior of animals appeared in 1980's[15, 16, 14, 17]. These models basically employ a somewhat similar strategy, but the one proposed by Reynolds[14] became most well-known. In the so-called "boid" model, the

individuals' motion is simulated by taking into account three rules: collision avoidance, velocity matching, and cohesion (or, according to Reynolds' original terminology, "flock centering"). These three rules can be implemented as repulsive, ferromagnetic, and attractive interactions, respectively, with other individuals that are within spherical zones, centered at the boid, with some radii, which can be different between the interaction types. Using this model, Reynolds showed that plausible flocking behaviors are reproduced; however, he did not apply much quantitative analysis because his primary intention was to construct a model for computer animation.

A systematic investigation of the boid model was carried out by Couzin et al.[18]. Their formulation of the behavioral rules are described in the following difference equations with discrete time steps and synchronous updates. At each time steps, each individual determines a desired direction of motion $\hat{\mathbf{d}}_i(t)$ by evaluating position and velocity of neighbors within three non-overlapping zones $\mathcal{S}_\mathrm{r}$, $\mathcal{S}_\mathrm{o}$, and $\mathcal{S}_\mathrm{a}$. If others are found in "zone of repulsion" $\mathcal{S}_\mathrm{r}$, a sphere of radius r_r centered on the position $\mathbf{r}_i$ of the individual i, the desired direction at next time step is chosen as

$$\hat{\mathbf{d}}_i(t+\Delta t) = -\hat{\mathbf{n}}\left(\sum_{\substack{j\in\mathcal{S}_\mathrm{r}\\ j\neq i}} \frac{\mathbf{r}_{ij}}{|\mathbf{r}_{ij}|}\right), \tag{1.1}$$

where $\hat{\mathbf{n}}(\mathbf{x}) = \mathbf{x}/|\mathbf{x}|$ is a vector normalization function and $\mathbf{r}_{ij} = \mathbf{r}_j - \mathbf{r}_i$ is the relative position between particle i and j. If no other individuals are present in $\mathcal{S}_\mathrm{r}$, then neighbors in "zone of orientation" $\mathcal{S}_\mathrm{o}$ and "zone of attraction" $\mathcal{S}_\mathrm{a}$, spherical ranges of $r_\mathrm{r} \leq \mathbf{r}_{ij} < r_\mathrm{o}$ and $r_\mathrm{o} \leq \mathbf{r}_{ij} < r_\mathrm{a}$, respectively, are considered:

$$\hat{\mathbf{d}}_i(t+\Delta t) = \hat{\mathbf{n}}\left(\sum_{j\in\mathcal{S}_\mathrm{o}} \frac{\mathbf{v}_j}{|\mathbf{v}_j|} + \sum_{\substack{j\in\mathcal{S}_\mathrm{a}\\ j\neq i}} \frac{\mathbf{r}_{ij}}{|\mathbf{r}_{ij}|}\right), \tag{1.2}$$

where $\mathbf{v}_i$ denotes the velocity of particle i. In the case that the sum of the vectors yields zero vector, or that no neighbors are in the range, then $\hat{\mathbf{d}}_i(t+\Delta t) = \hat{\mathbf{d}}_i(t)$. After incorporating the error effect, realized by a random rotation of $\hat{\mathbf{d}}_i(t+\Delta t)$ by an angle taken from Gaussian distribution, the velocity is updated in such a way that the speed is constant and the direction rotates itself towards $\hat{\mathbf{d}}_i(t+\Delta t)$ with a constant turning rate.

By changing the width of the behavioral zones, Couzin and coworkers found

transitions between four distinct modes of flocking, which they labeled as swarm, torus, dynamic parallel group, and highly parallel group. These modes are characterized by two order parameters: group polarization,

$$M(t) = \frac{1}{N}\left|\sum_{i=1}^{N} \mathbf{v}_i(t)\right|, \tag{1.3}$$

and group angular momentum,

$$L(t) = \frac{1}{N}\left|\sum_{i=1}^{N} \mathbf{r}_i^{\mathrm{c}}(t) \times \mathbf{v}_i(t)\right|, \tag{1.4}$$

where $\mathbf{r}_i^{\mathrm{c}} = \mathbf{r}_i - \sum_{j=1}^{N} \mathbf{r}_j$ is the relative position to the center of mass. The sharp transition and hysteresis phenomena are discussed with possible connection to the collective response and collective memory of fish school behavior.

Recently, Mototake and Ikegami[19] performed large scale simulations of the boid model using GPGPU based parallelization method. While the previous results are based on the numerical simulation with $N = 100$, qualitatively different behaviors are observed when the population size is increased up to the order of $N = 10^5$. The system does not end up in one of the four dynamical modes, but spontaneously forms a complex dynamic structure where a dozen of large swarming clusters are interconnected by filamentous streams. The origin of this "more is different" phenomenon has not be fully understood.

1.2.2 Vicsek model

Although the boid model displays rich collective behaviors, it is difficult to develop a quantitative understanding on the simulation results, because of the complexity of interactions and too many control parameters. Even if we keep the model minimum as possible, one has to adjust strength and range of three different interactions, determine the self-propelling speed and, possibly, the noise strength too. Variables can be made dimensionless by adopting one of interaction ranges as the unit of length and one of the interaction strengths or the self-propelling speed as unit of velocity, but the rescaled equations still have five or six parameters to be tuned.

The model proposed by Vicsek et al.[20], which assumes only the alignment with nearby individuals, can be regarded as the simplified version of the boid model. In the Vicsek model, individuals are modeled with point particles that drive themselves with a constant speed v_0 while interacting with other particles

in the spherical proximity $\mathcal{S}_i$. The dynamics is described as follows:

$$\mathbf{r}_i(t+\Delta t) = \mathbf{r}_i(t) + \mathbf{v}_i(t+\Delta t)\Delta t, \tag{1.5}$$

$$\mathbf{v}_i(t+\Delta t) = v_0 R_\eta \hat{\mathbf{n}} \left(\sum_{j \in \mathcal{S}_i} \mathbf{v}_j(t) \right). \tag{1.6}$$

where R_η denotes a rotation matrix that rotates vectors by a random angle chosen from a uniform distribution of amplitude $2\pi\eta$ (for 2D) or $4\pi\eta$ (for 3D).

A slightly modified version of the Vicsek model was proposed by Grégoire and Chaté[21]. The model employs a different manner to incorporate the noise to the dynamics, namely replacing Eq. 1.6 by

$$\mathbf{v}_i(t+\Delta t) = v_0 \hat{\mathbf{n}} \left(\sum_{j \in \mathcal{S}_i} \mathbf{v}_j(t) + \eta \mathcal{N}_i \xi \right), \tag{1.7}$$

where ξ denotes a random unit vector and $\mathcal{N}_i$ is the number of particles in $\mathcal{S}_i$. This modification reflects two different perspectives on where the errors stem from: the standard model assumes errors arise when the individual decides its next move from the perception of other individuals, while the modified model is based on the idea that the individual makes errors in the process of cognition and assessment of others. The treatment of the noise in the modified version is referred to as "vectorial" noise, contrasted with "angular" noise in the standard model.

Many-particle simulations indicate the Vicsek model presents some characteristic properties. First, ordered motion, in which particles moves into the coherent direction, emerges at high densities with small noise amplitude. The discovery of true long-range order in the two-dimensional Vicsek model was surprising to the physicists, because the Mermin-Wagner (MW) theorem forbids any long range order in two-dimensional equilibrium systems breaking a continuous symmetry at finite temperatures (which is equivalent to the existence of noise). Therefore, the violation of the MW theorem is thought to be due to the nonequilibrium nature of the model. The order-disorder transition as a function of density and noise amplitude is characterized by polar order parameter (Eq. 1.3). It was first thought that the transition is continuous[20]; however, a careful inspection with larger systems revealed that the transition is of first-order[21, 22]. To be more precise, there is a third phase, between the disordered phase and the full-order phase, that involves a long wavelength instability and phase separation[23]. In this regime, particles form dense and

ordered traveling bands (or, in three-dimensional case, sheets) that span vertically to the direction of motion. Outside the band, the particles are sparse and not aligned. The fact that this instability becomes noticeable only in systems sufficiently larger than the wavelength have brought a controversy over the nature of transition, but it is now a common understanding that finite-size effects and boundary conditions has a critical effect. One may say that this is another example of "more is different."

Another self-emerging property of the Vicsek model is anomalous density fluctuations in the system, which was theoretically predicted from symmetry arguments in pioneering works by Toner and Tu[24, 25]. Consider a box of volume V in the system. The number of particles inside the box at time t is denoted by $N(t)$. In a thermal equilibrium system off the phase transition, the time average $\langle N \rangle = \frac{1}{T}\int_0^T N(t)\mathrm{d}t$ and the variance $\Delta N^2 = \left\langle \left(N(t) - \langle N \rangle\right)^2 \right\rangle$ should scale as $\Delta N^2 \sim \langle N \rangle$ in the limit of $N \to \infty$. For Vicsek model, however, the fluctuation is greater than that, namely, $\Delta N^2 \sim \langle N \rangle^\alpha$ with $\alpha \simeq 1.6$ in both two and three dimensions. This so-called giant number fluctuations is observed for the broader class of active particle numerical models such as active nematics[26, 27] and self-propelled rods[28], as well as experimentally in bacterial systems[29] and vibrated grains[30, 31]. It is now considered to be a shared feature of active systems in Vicsek class[32].

1.2.3 Social force model

Developing mathematical models that describe pedestrian movement has long been considered to be of great importance for urban planners, architectural designers, and local administrators, who want to ensure the public safety while improving the efficiency of urban traffic. Since the first formulation of such model, which is inspired by fluid dynamics[33], continuum-based approaches have been improved and are still employed[34]. Although continuum modeling offers a certain advantage in simulating high-density flows, it has difficulties in addressing the motion of individual pedestrians because the details of the interaction between them are neglected. This is the reason microscopic models are called for.

Two classes of microscopic pedestrian models have attracted attention of physicists. In cellular automata (CA) models, time and space are discretized. Each pedestrian occupies a single site in a grid at each time step and hops to one of the neighboring sites at the next time step with certain probabilities. For this properties, CA models are often referred to as "rule-based." On the other hand, there are a group of "force-based" models, which assume that the space is continuous and describe individual's motion by a set of differential

equations. Readers may notice at this point that the force based models are constructed in the similar spirit with the boid model and the Vicsek model.

One of the most popular force-based models is introduced by Helbing and Molnár[35], assumes that the behavior of pedestrians is influenced by socio-psychological forces and governed by Newtonian dynamics. Each pedestrian i move towards the destination point $\mathbf{o}_i$; the heading vector (desired direction) is given by the difference from the current position,

$$\hat{\mathbf{d}}_i = \frac{\mathbf{o}_i - \mathbf{r}_i}{|\mathbf{o}_i - \mathbf{r}_i|}. \tag{1.8}$$

While being self-propelled toward the direction of $\hat{\mathbf{d}}_i$, the agent is influenced by socio-psychological forces $\mathbf{f}_{ij}$ from other individuals j, and follows a Newtonian dynamics, which is,

$$\frac{\mathrm{d}\mathbf{r}_i}{\mathrm{d}t} = \mathbf{v}_i(t), \tag{1.9}$$

$$\frac{\mathrm{d}\mathbf{v}_i}{\mathrm{d}t} = \alpha\hat{\mathbf{d}}_i(t) - \beta\mathbf{v}_i(t) + \sum_{j\neq i}\mathbf{f}_{ij}. \tag{1.10}$$

Here, α is the intrinsic self-propulsion force and β represents the quickness of relaxation to the individual's "natural" walking speed α/β. We assume that these coefficients take the same value for all the individuals, but they can differ from person to person with an appropriate distribution. Specific forms of the interaction force are slightly different between the literatures, but the most simple one is expressed by the form of exponential decaying function against the distance of two individuals,

$$\mathbf{f}_{ij} = A\exp\left[-\frac{|\mathbf{r}_{ij}|}{B}\right]\frac{\mathbf{r}_{ij}}{|\mathbf{r}_{ij}|}. \tag{1.11}$$

It is also possible to reflect other effects that arise from psychological and physical constraints, such as collision avoidance with obstacles and walls, the tendency of pedestrians to react more strongly to what happens in front of them, the tendency to give way more quickly to those approaching at a high rate of speed, and the repulsion between individuals at physical contact in dense crowd[36, 37].

One can test the validity of the models or calibrate their parameter values by the degree of agreement between the simulation results and the empirical data. The comparison can be made in three different levels. One can either look into (i) the microscopic quantities, namely, trajectory of single hu-

man movement and paths of two people takes when they are passing each other; (ii) the macroscopic quantities such as flow rate, density profile, and the fundamental diagram, which expresses the relationship between the flow and the density. (iii) The ability to reproduce qualitative traits, especially the self-organized patterns introduced in the previous section, is also often emphasized. The social force model, along with its variants and other force-based models, is successful in describing the single pedestrian movement, as well as reproducing some of the collective phenomena such as lane formation, clogging and intermittent oscillatory flow at bottlenecks. However, the stop-and-go waves and crowd turbulence observed at high densities are not derived from the social force model, and there has been a claim that underdamped dynamics described by second order differential equations leads to unrealistic oscillatory behaviors and therefore fails to account for the emergent phenomena[38].

1.3 Scope of the thesis

We briefly introduced in the previous sections the examples of collective motion observed in the real world, as well as the three basic mathematical models, all of which employ the idea of *self-propelled particles*, regardless of whether their advocates referred to the concept at the time of proposal. It has become a common belief among the researchers in the field in the past two decades that the conceptual framework of collective motion of self-propelled particles is based not merely on the apparent similarities between various phenomena, but on the universality that does not depend on the details of the systems. This justifies to study the properties of simplified models, like the Vicsek model, which does not directly provide an exact expression of the microscopic elements of any physical, biological or social systems and therefore does not lead to precise prediction on the behavior of the systems, and to still think that the analysis of such models can contribute to the understanding of the emergent phenomena.

In the past two decades, the Vicsek model and its variants have been considered to be one of the minimal self-propelled particle models, and subjected to the intensive investigation. As stated above, it resulted in the understanding of the features shared in the so-called Vicsek universality class, which is defined by the local alignment between particles, or ferromagnetic interactions. Nevertheless, empirical findings suggest that the Vicsek-type interaction is hardly found in its pure form in real systems:

- *Fish.* From the observation of fish school in a shallow pools, Gautrais et al.[39] concluded that fish follow a set of behavioral rules that resembles

the boid model. However, the implementation detail is different from Couzin et al.[18]: The force acts not on the position or heading but on the angular velocity of each particles.

- *Birds.* Ballerini et al.[40] analyzed 3D reconstructed image of starling flocks to find that the birds interact with others in topological neighborhood, i.e., n nearest neighbors, rather than those in metric neighborhood (within a sphere of radius r).

- *Bacteria.* In spite of recent experimental developments on bacterial collective dynamics, the specification of interaction remains elusive. Many model bacteria such as *E. Coli* and *B. subtilis* has an elongated shape, which makes the interaction anisotropic. The excluded volume effect often results in the effective nematic interactions, and the flagellar bundling and long-range hydrodynamic forces are believed to govern their dynamics too[2, 41].

- *Eukaryotic cells.* Eukaryotic cells are mechanically connected to each other through junctions mediated by receptors called as cadherins. This cell-cell adhesion facilitates the collective cell migration and position rearrangements[8, 42].

- *Human pedestrians.* Aside from the social force model, several force-based models for pedestrian movement have been proposed, including the centrifugal force model[43, 44], which incorporates dependence of the interaction on velocity. Recently, Karamouzas et al.[45] found from an analysis of crowd data sets that interaction between pedestrians are governed by an "anticipatory" force: People are subject to repulsive forces which have a power-law dependence on the length of time until the moment they expect to collide with each other.

One can easily see from the above examples that the interactions between components in biological systems are diverse, complex, situation dependent, and sometimes hard to identify by observational methods. The difficulties can arise either from the process of obtaining data or from the process of interpreting it. Birds and large mammals must be studied in the field, and therefore reconstruction of individuals' three dimensional positions in large groups can be demanding. Recent developments in video tracking technology[40, 46, 47, 48] and biologging devices using GPS and acceleration sensors[49] are helping researchers to make use of the data with high resolution in time and space. Fish schools are studied in natural environment using sonar and echosounder[50],

as well as in the laboratory tanks[51, 52, 53, 54]. The former has limitation in tracking the individual movement, while the latter suffers difficulties in handling a large population and in getting rid of the effects of tank shapes and boundary walls. Compared to other animals, the empirical data of human pedestrian dynamics are much more accessible, because it is possible to perform controlled experiments in various environments[11, 12], except for extreme situations where the crowd density are high enough to cause a mass disaster[13]. However, the fact that there are a number of mathematical models that seem to have similar ability to explain the empirical results implies that inferring the hidden structure of interactions and constructing a proper model is not a straightforward task, even if we are provided with abundant data.

In this regard, the universality of the collective motion should be pursued both by empirical approach and by the means of abstract modeling. It is particularly important to understand how the difference in interaction types leads to the difference in collective behaviors of the system, and what details are relevant for assessing whether two different models fall into a same universality class or not.

The Vicsek model can be considered as a subversion of the Reynolds' boid model that assumes only one of the three interaction rules—the alignment—while ignoring the other two, the repulsion and the attraction. This perspective naturally leads to the following questions: What if we assume purely repulsive or purely attractive SPPs? Do those systems exhibit a different behavior from the collective motion of the Vicsek particles? What are the roles of the two types of interactions in the flocking phenomena?

Purely repulsive SPP is of particularly interest because there are strong empirical evidences supporting that repulsion plays an important role: The social force model[35] and the anticipatory power-law model[45] assume that the human behavior is governed by repulsion; the collective motion of keratocyte cells is described by repulsive dynamics; apart from biological systems, vibrated grains[30, 55] and active colloidal particles[56] interact with others through excluded volume. Pure attraction, on the other hand, is not found in the real systems, although a purely attractive SPP model is studied by Strömbom[57].

Repulsive SPP Models are studied in previous literatures[58, 59, 60, 61], although they focus on the collective motion under particular conditions; therefore a systematic understanding on the behavior of the system has been lacking. The work by Hanke et al.[62] was the first example to scrutinize the collective behavior of a repulsive SPP model, but this model has a certain limit

in explaining the collective motion seen in real systems, as explained in the next Chapter. In order to overcome these points, we construct a simple and general repulsive SPP model which aims to bridge or expand some of the previous approaches. By performing an extensive investigation on the dynamic properties the model displays, we try to set a much broader perspective on the universality behind the flocking systems.

1.4 Outline

This thesis is organized as follows.

Chapter 2 introduces the two-dimensional repulsive SPP model. By implementing particle dynamics simulations, we numerically explore the behaviors of the multi-partice systems. The transition from disordered state to ordered state is studied by investigating the properties of the order parameter dynamics and density fluctuations.

Chapter 3 discusses the microscopic origins of the ordering behavior. The Boltzmann formalism is introduced to derive the mesoscopic description of the dynamics. We demonstrate that binary collision and scattering process is responsible for the emergence of the coordinated motion. We verify the validity of the theory for a dilute limit and for finite densities.

Chapter 4 turns to the collective motion of repulsive SPPs in the geometries different from the system with periodic boundary conditions. Three geometries are particularly considered: the "pipe" geometry, where system is bounded in one direction while periodic in the other, and the "box" and the "disk" geometries, where the system is enclosed by reflecting walls. Particular attention is paid for the lane formation phenomenon in a pipe. We study how the spontaneously formed lane structure is affected by the finite memory of pedestrians.

Chapter 5 reports the main conclusions and discussion for future works.

Chapter 2

Repulsive self-propelled particles

2.1 Introduction

Following the seminal works by Vicsek et al.[20] and Toner and Tu[24, 25], the interest of physicists in collective motion of self-propelled particle (SPP) systems has been growing in past two decades. A well established approach in the field is the Vicsek-type SPP model[20, 21, 22], as introduced in Chapter 1. It assumes the particles drive themselves with a constant speed while adjusting their direction of motion parallel to their neighbors' velocities. It has been shown that the non-equilibrium character of the systems leads to development of long-range order and giant density fluctuations, which are unusual in equilibrium systems[24, 25, 26, 27].

Experiments using vibrated grains and driven colloids[30, 31, 55, 63, 56, 64] suggest that the similar properties can also be found in non-living systems. However, the Vicsek model is not likely to illustrate the microscopic nature of these systems, where particles do not "compute" the average of their neighbors' velocities. It is rather natural to assume that the elements interact with repulsion through excluded volume.

Previously, Hanke et al.[62] proposed a model of soft, repulsive active particles, explored its collective behavior over parameters, and found that a polarized state emerges at a certain parameter region. However, their model has some inconsistencies at the microscopic level when compared to actual granular or colloidal matter. First, the particles are not always as soft and strongly overdamped as the model requires them to be in order to achieve the collective motion. Second, the origin of the noise is unclear, since thermal fluctuation is not relevant in the length scale we deal with.

In this Chapter, we first construct a simple repulsive self-propelled particle model. The periodic boundary conditions are employed to investigate the bulk properties.

2.2 Model

2.2.1 Principles

First, let us discuss about what are the key elements to construct the self-propelled particle model.

- *Order of dynamics.* By definition, the SPPs must present self-propulsion, which can be treated in many different ways depending on the model. It can be incorporated as a self-propelling velocity in a continuous-time first-order differential equation, i.e., $\dot{\mathbf{r}} = \mathbf{F}_{\mathrm{s}} + \ldots$, or in a discrete-time first-order difference equation, $\mathbf{r}(t+1) = \mathbf{r}(t) + \mathbf{F}_{\mathrm{s}} + \ldots$. From the viewpoint where the connection with the conventional Newtonian dynamics is emphasized, the self-propulsion is described as a force in a second-order differential equation, $\dot{\mathbf{v}} = \ddot{\mathbf{r}} = \mathbf{F}_{\mathrm{s}} + \ldots$. The first-order dynamics, sometimes referred to as "Aristotelian," can be regarded as an overdamped limit of the second-order Newtonian dynamics, where the self-propulsion and the dissipation are almost always balanced and the inertia can be neglected. Obviously the Vicsek model is an example of Aristotelian dynamics, while the boid model and the social force model are normally implemented to posses the Newtonian character.

- *Polarity.* Another classification can be made by whether the self-propulsion $\mathbf{F}_{\mathrm{s}}$ is defined by an internal degree of freedom or is exerted in a random manner. Usually, the biological agents have an preferred orientation of motion and drive themselves into that direction: we call it "polarity", following the terminology of cell biology. A simple implementation is to assume that the polarity is defined in the direction of motion, as in the Vicsek model. At the other extreme, the polarity can be a vector always pointing at a fixed spatial point in the system, or always pointing to the same direction (fixed vector); the assumption of the social force model that every pedestrian has a desired direction into their own destination makes the model fall into this class. A natural generalization that bridges these two extremes is to assume that the polarity does not necessary agree with the velocity nor is it fixed to a pre-defined direction, but

evolves with an "in-between" dynamics, where it has a tendency to align with the velocity while keeping a finite memory of its past headings.

- *Dry or wet?* One of the characteristics of the Vicsek model is that it assumes no momentum conservation for the inter-particle interaction. However, by considering that the particles are suspended in a fluid media, one can suppose that total momentum of the SPPs and the solvent is conserved. In this case the hydrodynamic interactions must be taken into account in the dynamics of model. These two classes—dynamics with and without momentum conservation—are referred to as "dry" and "wet", respectively[65]. In our study, we restrict ourselves to a dry model, where hydrodynamic flows can be neglected compared to the characteristic length scale of the system.

- *Repulsion.* The repulsive interaction between particles can be in various forms, depending on the model. For example, an implementation of the boid model assumes that the sum of repulsive forces from other particles located within a range is normalized when acting on the particle[18]. The social force model adopts the exponentially decaying potential, which is asymmetric towards the desired direction and possibly has elliptical shape elongated in the direction of motion[35]. In both cases, Newton's third law is violated. If one is interested more in physical interactions than in social ones, the excluded volume will play an important role, as in Refs.[59, 60, 62]. Although a hard-core potential is the simplest (requires no parameter) form to model the excluded volume effect, it is not algorithmically compatible with nonlinear equations of motion. Therefore, we employ a soft-core potential with relatively large stiffness.

- *Stochastic or deterministic?* Almost all the mathematical SPP models incorporate some kind of noise in the dynamics. In many cases, the noise level plays the role of the temperature in equilibrium systems and becomes the control parameter to induce a phase transition. Still, the origin of the noise in SPP systems is unclear. In traditional equilibrium systems, the noise stems from thermal fluctuations. In most SPP systems, however, thermal fluctuations are hardly significant compared to the characteristic length scale of the system. Hydrodynamic origin is another candidate, but its effect is negligible in low fields. The most probable hypothesis is that intrinsic errors and uncertainties of biological agents during their perception and decision making process lead to the stochastic behavior. Plausible as it may seem, the problem is that we know little about the nature of the noise: whether it follows an uniform

distribution or Gaussian, whether it is additive or multiplicative, scalar or vectorial as has been discussed for the Vicsek model, if it is correlated in time and space or not, etc. These differences can drastically change the behavior of the system. For example, assuming time-correlated noise leads to the formation of vortex observed in microtubule assay[66]. Since our primary motivation is not on exploring the effect of noise, we would rather employ deterministic dynamics.

2.2.2 Formulation

We consider N disk particles of equal radius a in a two-dimensional continuous surface. The dynamics is governed by the following deterministic equations:

$$\frac{\mathrm{d}\mathbf{v}_i}{\mathrm{d}t} = \alpha\hat{\mathbf{e}}(\psi_i) - \beta\mathbf{v}_i + \sum_j \mathbf{f}_{ij}, \tag{2.1}$$

$$\frac{\mathrm{d}\psi_i}{\mathrm{d}t} = \gamma(\theta_i - \psi_i). \tag{2.2}$$

Eq. (2.1) describes the Newtonian equation of motion with velocity $\mathbf{v}_i = \mathrm{d}\mathbf{r}_i/\mathrm{d}t$. The first term of the right-hand side is the self-propelling force of fixed magnitude α along the direction of the polarity, an internal degree of freedom defined by an unit vector $\hat{\mathbf{e}}(\psi_i) \equiv \cos\psi_i\hat{\mathbf{x}} + \sin\psi_i\hat{\mathbf{y}}$. The second term is dissipation proportional to $\mathbf{v}_i$, whose strength is determined by β. This term represents the friction from the environment, so β should be determined based upon the viscosity of the surrounding media. The stationary speed of the particle is given by α/β.

The interaction force is given by binary, short-ranged repulsion: Here we assume Hookean contact with stiffness k,

$$\mathbf{f}_{ij} = \begin{cases} -k\left(2a - |\mathbf{r}_{ij}|\right)\dfrac{\mathbf{r}_{ij}}{|\mathbf{r}_{ij}|} & (|\mathbf{r}_{ij}| < 2a) \\ \mathbf{0} & (\text{otherwise}), \end{cases} \tag{2.3}$$

where $\mathbf{r}_{ij} = \mathbf{r}_i - \mathbf{r}_j$.

Eq. (2.2) describes the time evolution of the polarity ψ_i. When ψ_i deviates from the direction θ_i of the velocity, it is rotated by a torque proportional to the deviation $\theta_i - \psi_i$ with a coefficient γ. Thus the equations include damping term for both translational and rotational degrees of freedom. The former is underdamped, while the latter is overdamped.

Note that each parameter gives a different characteristic time: $\tau_\alpha = 2a\beta\alpha^{-1}$ is the time scale that a particle at the stationary speed takes to run its own diameter; $\tau_\beta = \beta^{-1}$ is the relaxation time of speed; $\tau_k = k^{-1/2}$ is the characteristic time during which two colliding particles are in contact; and $\tau_\gamma = \gamma^{-1}$ is the relaxation time of polarity. Without loss of generality, we set unit of length and time as $2a = 1$ and $\beta^{-1} = 1$, and obtain rescaled equations.

2.3 Implementation methods and parameter choices

We perform particle dynamics simulations of a system consist of N particles in a square box of size $L \times L$ with periodic boundaries. Initial position and polarity of each particle are randomly assigned from uniform distributions. The random choice of the spacial configuration can result in large overlaps between particles. In order to avoid this unphysical situation, the position of the particles are adjusted, prior to each run, in such a way that dynamics assuming only the repulsive interaction potential reduces the overlaps. In this short time interval (usually $t \simeq 10$), the self-propelling forces are switched off, i.e., $\alpha = 0$.

Unless otherwise specified, we discuss the results for $\alpha = 1$ and $k = 100$. The maximum overlap ξ between particles is given by the balance between the self-propulsion α and the repulsion $k\xi$, in the case that we can ignore interaction with other particles. Under the present choice of parameter values, overlaps are less than 1% of the diameter, so the elasticity is large enough to avoid unphysical situations where particles in contact pass through each other.

A fourth-order Runge-Kutta method is employed for the numerical integration. The time step size is chosen to be sufficiently small (20 times smaller) compared to both τ_k and τ_γ, either of which defines the shortest time scale of the dynamics in the system.

One of the difficulties in the implementation of the molecular dynamics method is that a naive calculation of the interaction forces is computationally expensive. The force needs to be calculated for every particle pair, but the total number of pair grows as $O(N^2)$. For short-ranged interaction, a simple solution to this problem is to divide the system into small cells with a mesh size equal to (or larger than) the interaction radius, so that we only need to consider interactions between particles that belong to the same cell and adjacent cells (eight neighboring cells in 2D). This method accelerates the calculation up to the order of $O(N)$ for a fixed density, making large scale simulations possible.

2.4 Results

2.4.1 Ordering behavior

As shown in Fig. 2.1, the system exhibits polar ordering and large density fluctuation, the two characteristics also seen in the Vicsek model. The polar order is characterized by the average normalized velocity,

$$\mathbf{M} = \frac{1}{N}\sum_{i=1}^{N}\hat{\mathbf{e}}(\theta_i). \tag{2.4}$$

If the system is in random state $M = |\mathbf{M}| \simeq 0$, while $M = 1$ for a perfectly ordered state. In order to quantify the density fluctuation, we divide the system into N_c small cells of size 2×2 and take the standard deviation of the local packing fraction,

$$\Delta\phi = \sqrt{\frac{1}{N_c}\sum_{j=1}^{N_c}(\phi_j)^2 - \left(\frac{1}{N_c}\sum_{j=1}^{N_c}\phi_j\right)^2}, \tag{2.5}$$

where ϕ_j denotes the local packing fraction in the cell j.

Fig. 2.1 shows a typical ordering behavior. Initially, the system is randomized in position and in polarity, so both M and $\Delta\phi$ have small values. When the ordering starts, relatively dense and locally ordered regions appear and grow to form several clusters. The clusters eventually merge with each other until all the particles move into an identical direction. The time series of M and that of $\Delta\phi$ display a simultaneous increase. Fig. 2.2 – Fig. 2.5 shows the development of order parameter M and of density fluctuation (the variance ΔN^2 of the number of particles contained in subcells of different sizes). In ordered state, ΔN^2 scales as $\langle N\rangle^\delta$ with $\delta \simeq 1.9$, showing that the repulsive SPP model also exhibits giant number fluctuations. Exceptions can be found for the cases that $\gamma \ll 1$, where δ is significantly small.

2.4.2 Phase transition

We explore the behavior of the model by implementing a set of simulations with different packing fractions $\Phi = Na^2\pi/L^2$ and rotational damping parameter γ. We find that the globally aligned state emerges in the regime where system is dense and rotational damping is weak, while the disordered, isotropic state persists if we set the packing fraction small and the damping parameter large.

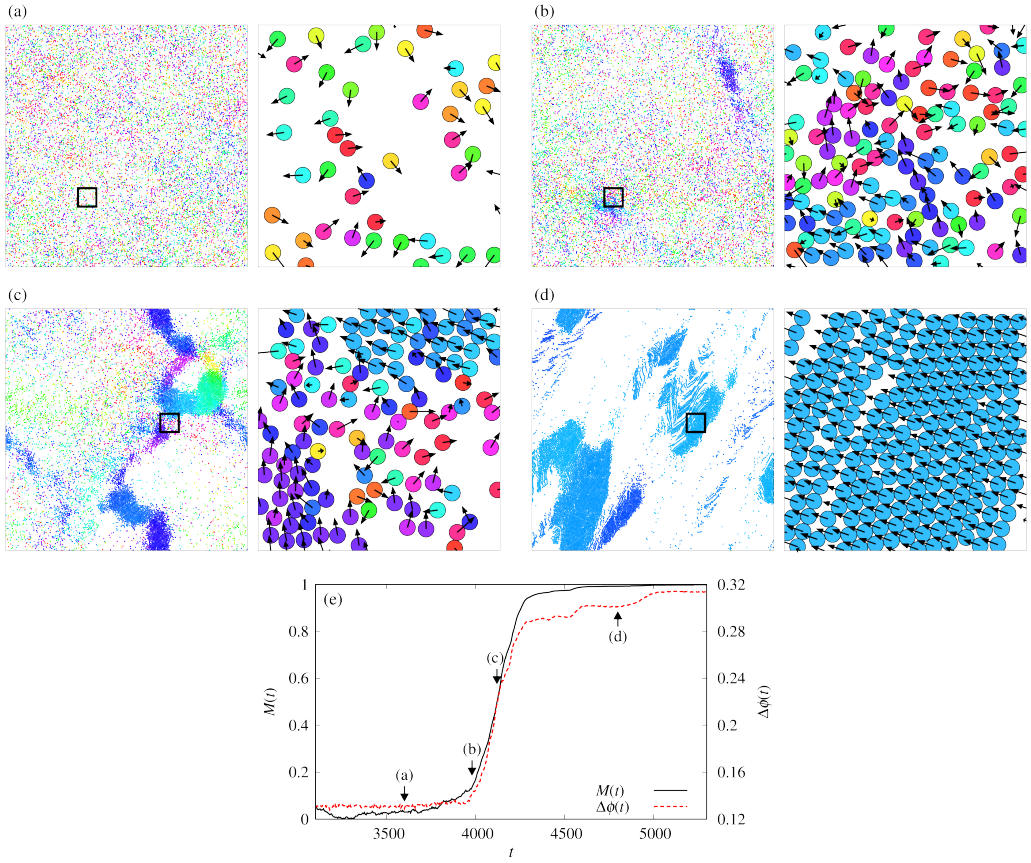

Figure 2.1: Ordering process observed in a representative run for $\Phi = 0.2$, $\gamma = 15.2$, a parameter set which is close to the phase boundary. (a–d) Snapshots of the system at different times. At each times, the whole system ($L = 198.2$) is on the left; enlarged image of boxed area of size 15×15 on the right. The arrows and the colors denote the direction of each particle's velocity. (a) $t = 3600$; the system is in isotropic, disordered state. (b) $t = 3980$; dense areas appear and local polar order grows within them. (c) $t = 4120$; several locally ordered clusters are formed. (d) $t = 4800$; the clusters eventually merge with each other until the whole system moves coherently. (e) Time development of the global polarization $M(t)$ and fluctuation in local volume fraction $\Delta\phi(t)$ from $t = 3100$ to $t = 5300$. Arrows correspond to the times in the top figure.

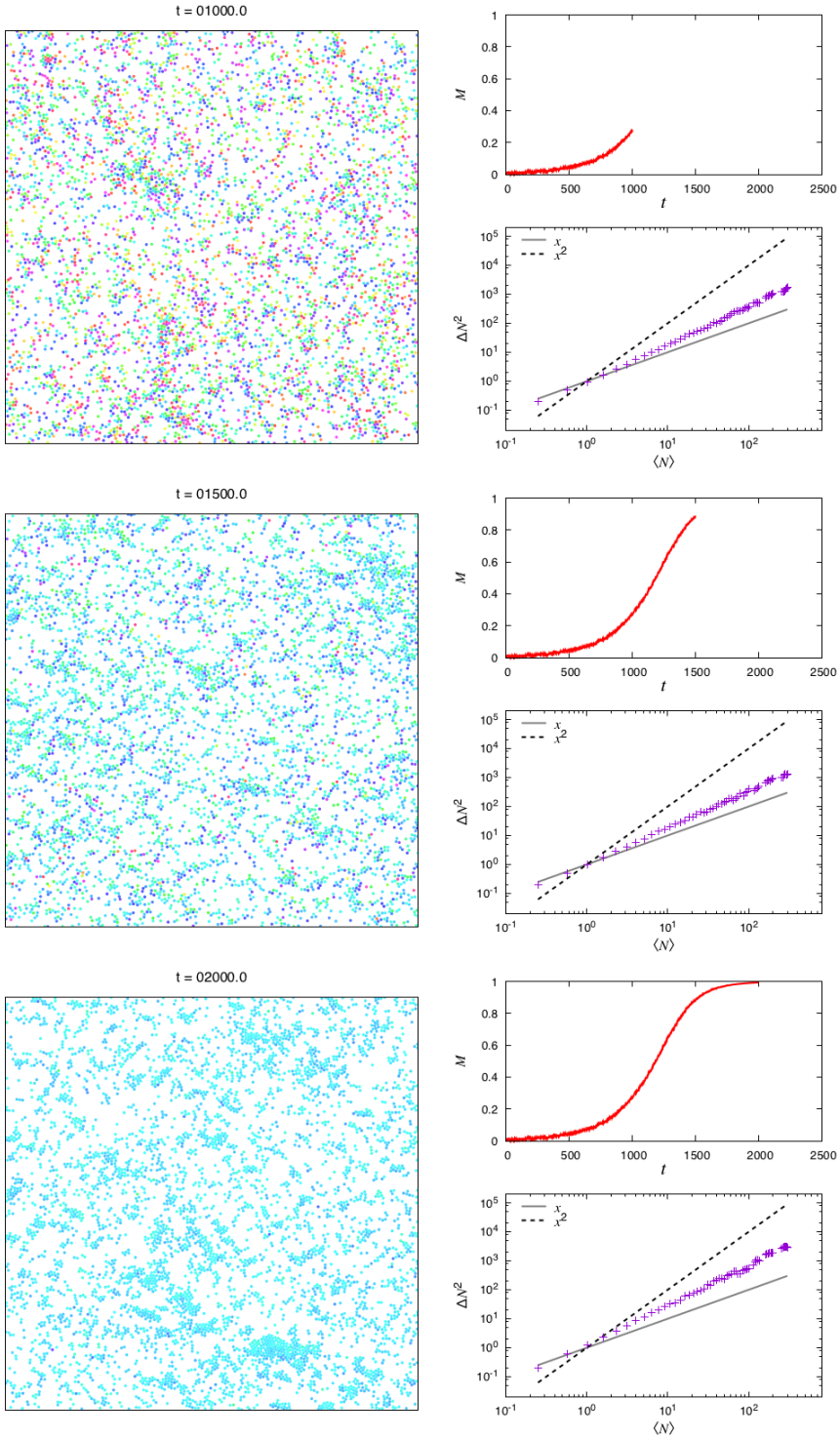

Figure 2.2: Instantaneous snapshots, development of order parameter and instantaneous density fluctuations in a representative run for $\Phi = 0.2$, $\gamma = 0.01$.

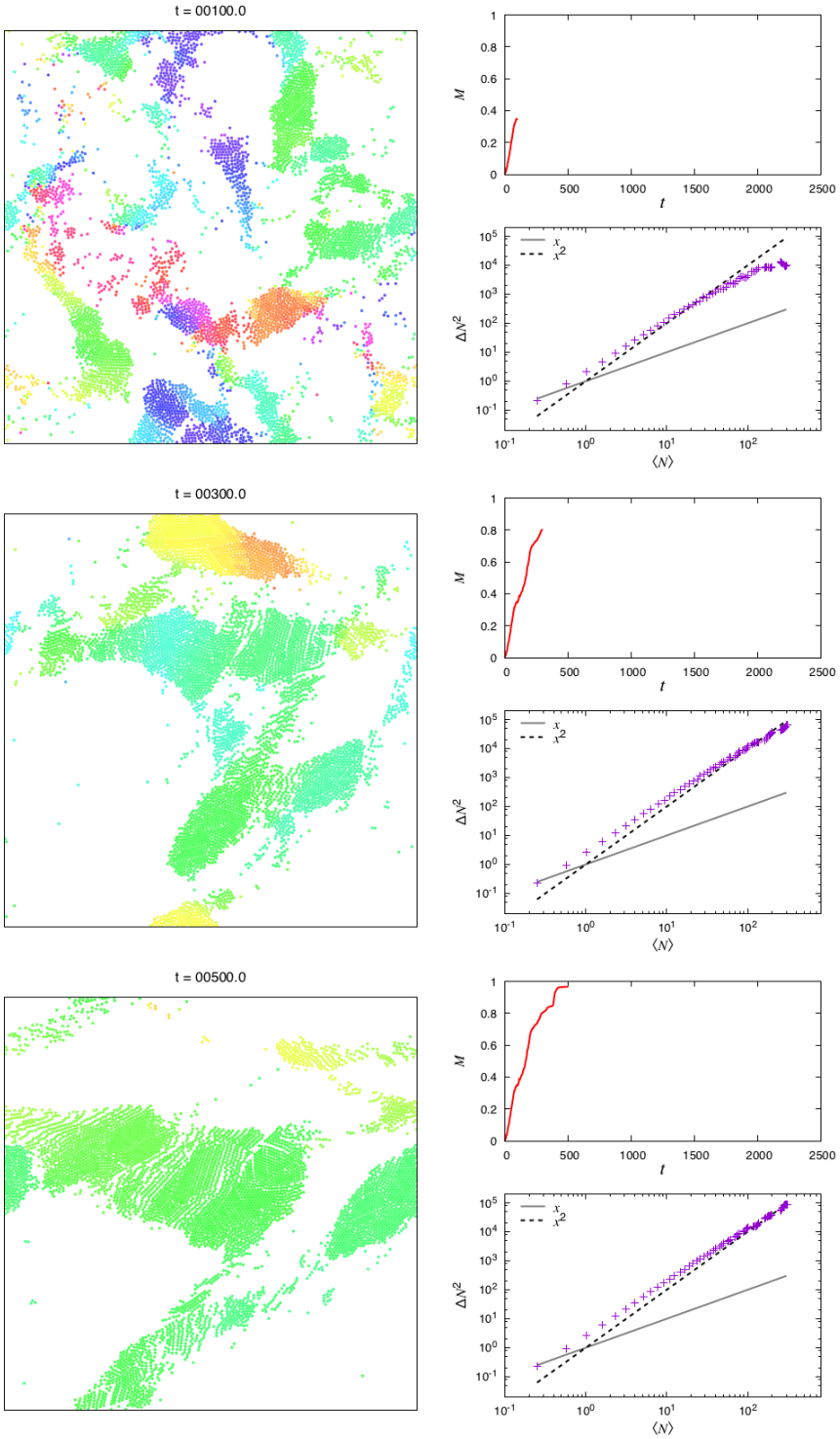

Figure 2.3: Instantaneous snapshots, development of order parameter and instantaneous density fluctuations in a representative run for $\Phi = 0.2$, $\gamma = 1$.

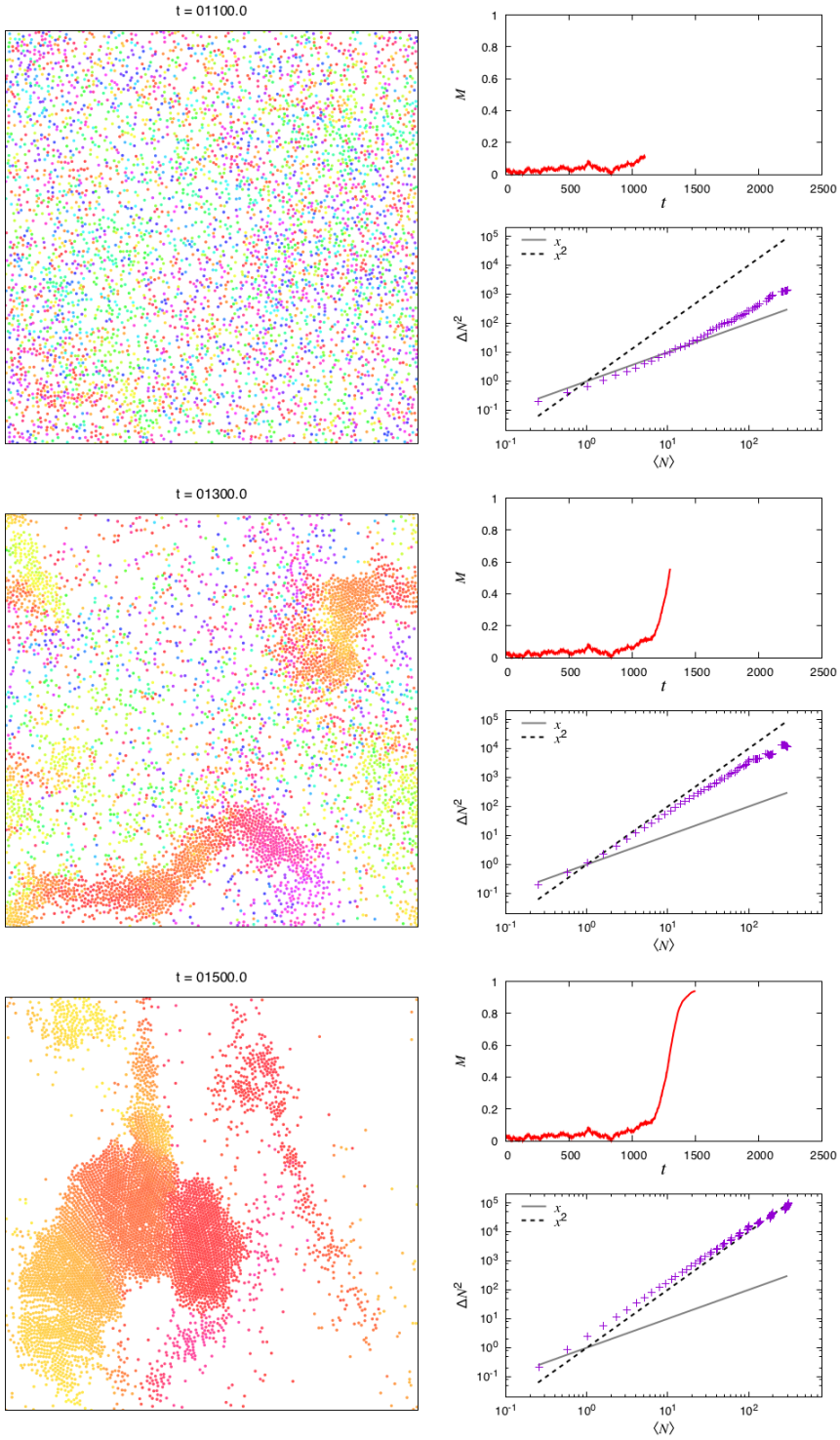

Figure 2.4: Instantaneous snapshots, development of order parameter and instantaneous density fluctuations in a representative run for $\Phi = 0.2$, $\gamma = 14.5$.

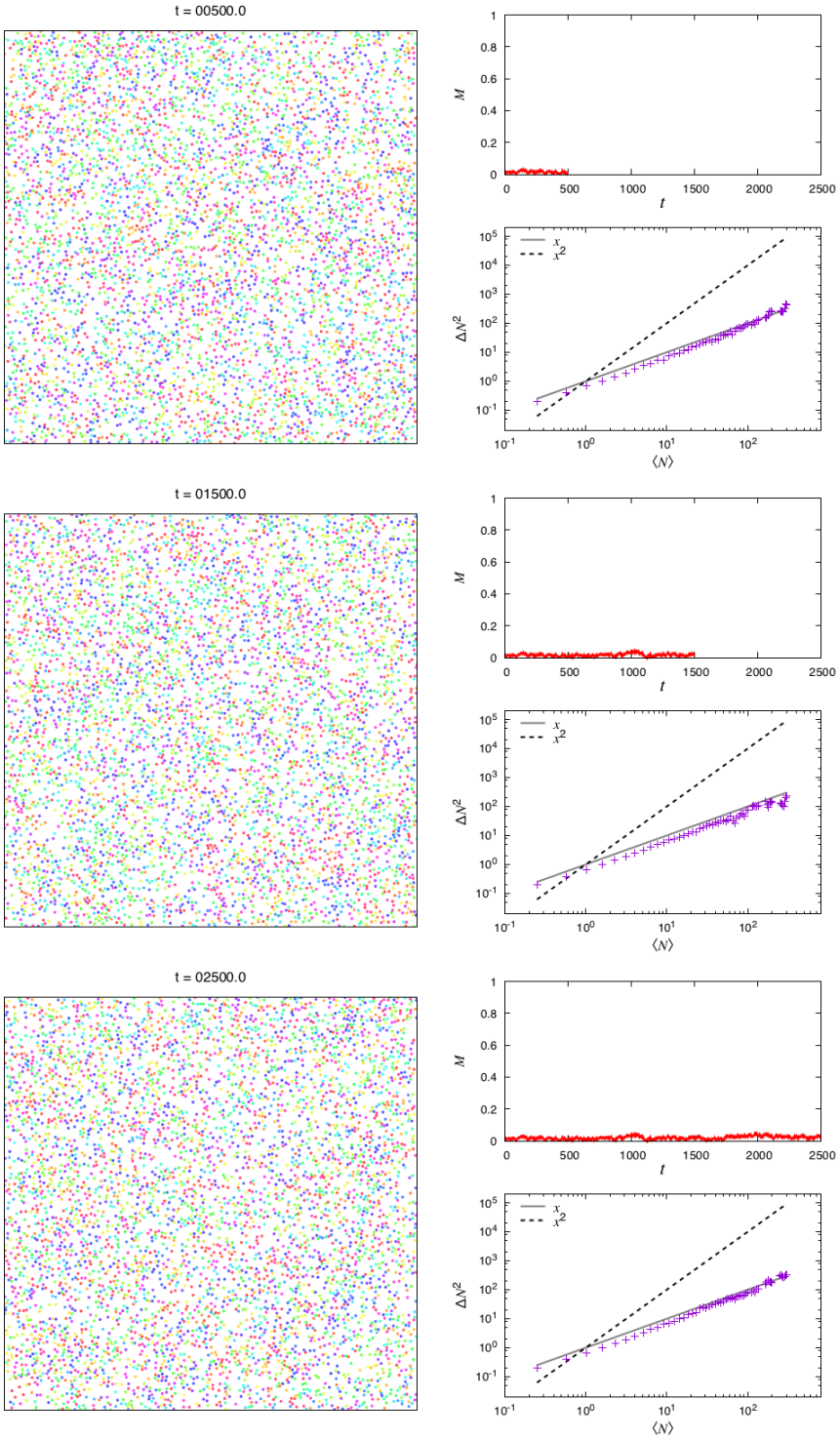

Figure 2.5: Instantaneous snapshots, development of order parameter and instantaneous density fluctuations in a representative run for $\Phi = 0.2$, $\gamma = 20$.

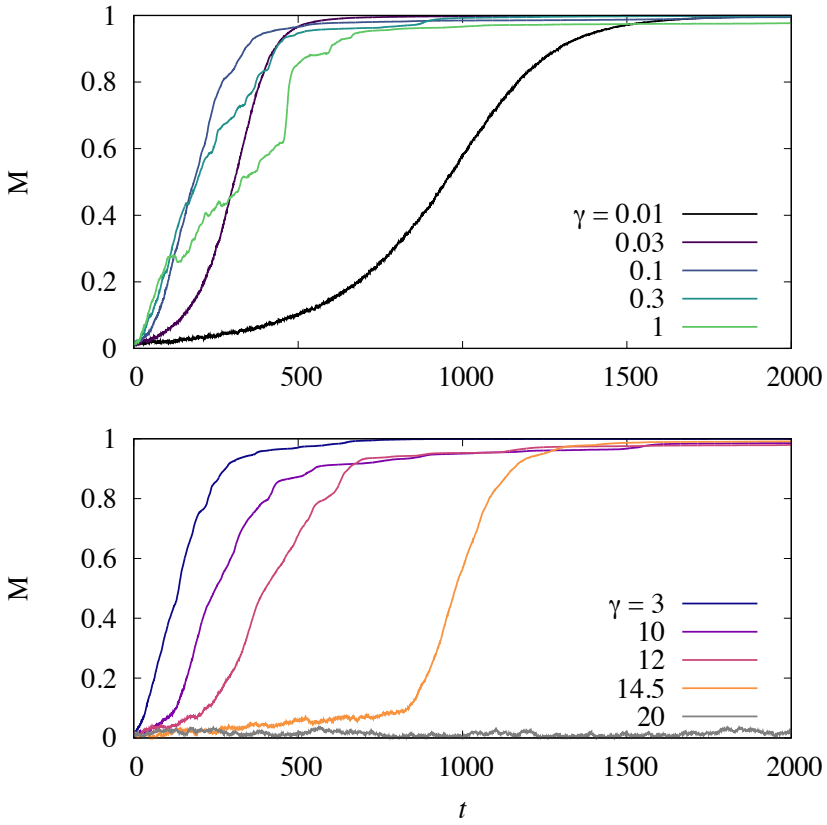

Figure 2.6: Representative time series of the global polarization $M(t)$ for various values of γ. As γ is increased, the order growth becomes faster for the regime of $\gamma < 1$; the waiting time until ordering becomes larger for $\gamma > 1$, especially near the transition point, and finally the system does not exhibit ordering behavior within the simulation time. The parameters are $N = 10000$ and $\Phi = 0.2$.

For $\gamma = 0$, where polarities are never rotated from initial randomized condition, the system maintains a trivial disordered state; however, a small but finite value of γ leads to a slow ordering. Representative time developments of the global polarization are shown in Fig. 2.6.

We construct the phase diagram by performing a set of runs (typically 8 to 16) with different initial configurations for a certain simulation time T. If polar order, namely $M > 0.8$, is established for one run or more, then the parameter set is classified as a part of ordered region; otherwise, it is in the disordered phase. We choose $N = 10000$ and $T = 5000$ (Fig. 2.7).

In the ordered region near the phase boundary, the system maintains the

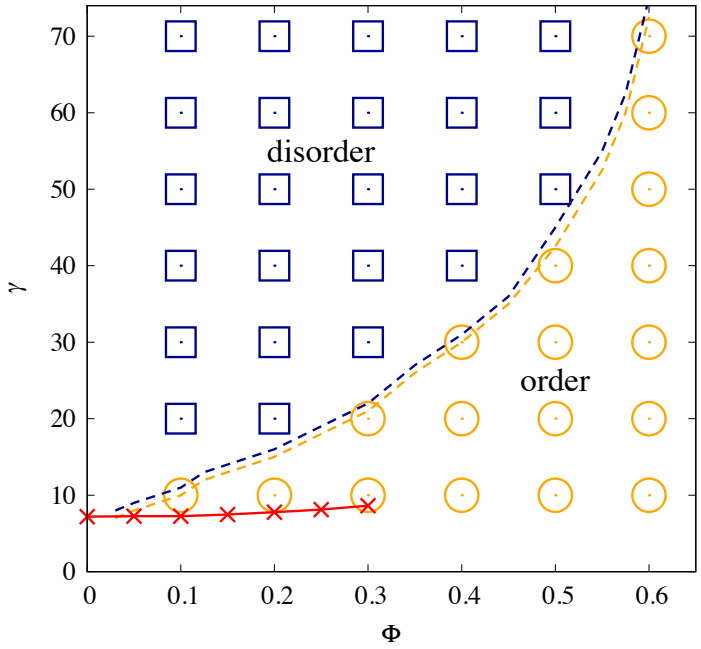

Figure 2.7: Phase diagram as a function of packing fraction Φ and damping parameter γ. Orange circles indicate parameter sets where ordered final state is observed at least for one run; blue squares are where the system remained disordered throughout the simulation time in all the realizations. Orange and blue dashed lines connect the uppermost points in ordered region and the lowermost points in disordered region, respectively, confirmed by a finer parameter search. Red crosses with solid line denote the zero-crossing points from the binary scattering analysis.

disordered state (small M) until it suddenly transits to the ordered state ($M = 1$). The lifetime t_w of the disordered state, which we refer to as the waiting time, varies depending on the initial configuration. As we increase γ, t_w tends to be longer and, eventually, ordering behavior does not take place within the simulation time for any realizations.

We look into the distribution that t_w follows for each parameter set (N, Φ, γ). In Fig. 2.8, the second central moment $\mu_2 = \langle (t_w - \langle t_w \rangle)^2 \rangle$ and third central moment $\mu_3 = \langle (t_w - \langle t_w \rangle)^3 \rangle$ are plotted against the average $\langle t_w \rangle$. In the large waiting time regime, namely where $\langle t_w \rangle > 5000$, two moments satisfy $\mu_2 = \langle t_w \rangle^2$ and $\mu_3 = 2\langle t_w \rangle^3$, which is expected for exponential distributions. The fact that the waiting time follows an exponential distribution implies that ordering events occur as Poisson processes involving nucleation phenomena.

Next we discuss how the phase diagram would be changed if we choose other

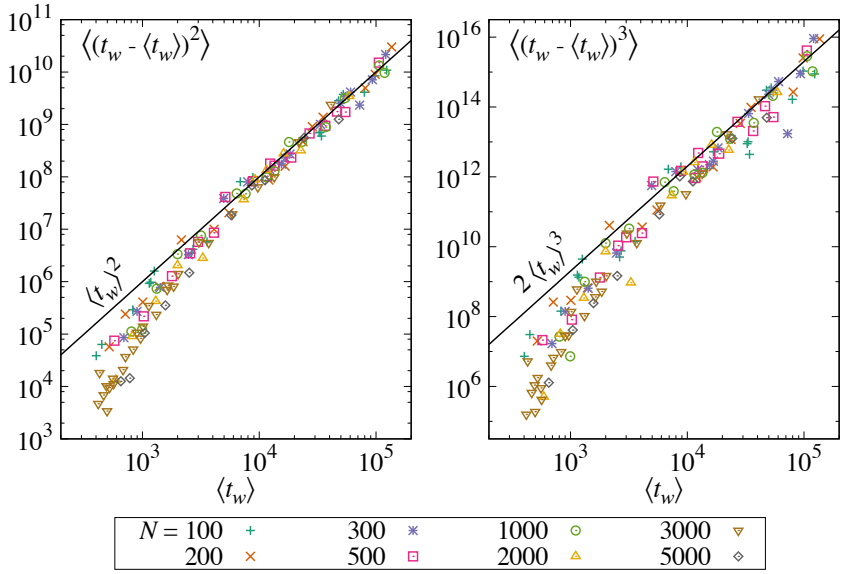

Figure 2.8: Average waiting time $\langle t_w \rangle$ versus the variance (left) and $\langle t_w \rangle$ versus the third central moment (right). The straight lines represent the expected relations between the moments for exponential distributions.

system sizes and time scales. Finite-size effects are investigated by changing the number of particles N while keeping the volume fraction Φ fixed. In small systems, $\langle t_w \rangle$ strongly depends on N; in larger systems, however, the increase becomes insignificant (Fig. 2.9, inset). We confirm that $N = 3,000$ is sufficiently large to avoid the finite-size effects for the time scale that we deal with.

$\langle t_w \rangle$ displays a rapid increase as a function of γ (Fig. 2.9). It is difficult to identify the function that fits the growth, but a phenomenological double-well potential picture, which will be described in the next subsection, implies that the ordering behavior can occur in any parameter region if we wait long enough. If this is the case, the phase classification inevitably depends on the observation time. Fortunately, the rapid increase, which seems to be exponential or faster, also ensures that the results with an moderately long simulation time provide a good approximation of the results with longer time scales. In other words, the phase diagram would be changed only slightly even if an order of magnitude longer observation time is employed.

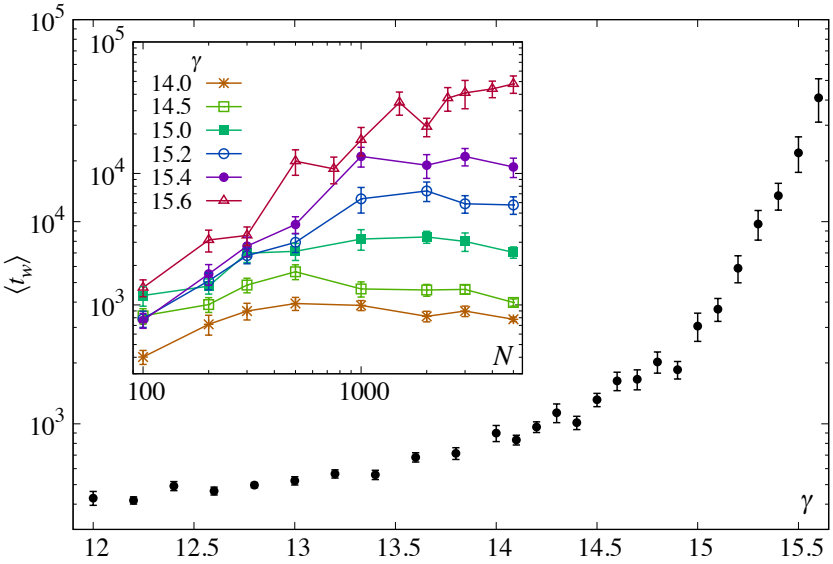

Figure 2.9: $\langle t_w \rangle$ for system of volume fraction $\Phi = 0.2$. The error bars represent the standard error. Main figure: Increase as a function of rotational damping parameter γ. The number of particles $N = 3000$. The onset of rapid increase is prominent around $\gamma \sim 14.5$. Inset: System size dependence for different values of γ.

2.5 Phenomenological theory on dynamics of order parameter

In this section, we show that the dynamics of the order parameter is described as a motion in a double-well potential. This phenomenological picture is consistent with the Poissonian character of the ordering process. It also provides a possible explanation for the divergence of the waiting time: In the ordered regime far from the boundary, the system quickly evolves from an unstable disordered state to an ordered state; near the boundary, however, the disordered state becomes metastable and a nucleation process is necessary to escape from it.

When the system is in the disordered state, the global polarization vector $\mathbf{M}$ fluctuates around $\mathbf{0}$. The microscopic origin of the fluctuation is change in polarity of the particles caused by collisions to their neighbors. We expect that the collision events are uncorrelated to each other, and the time development of $\mathbf{M}$ can be treated as Brownian motion in the potential. Assuming that the potential is harmonic around $\mathbf{M} = \mathbf{0}$, we expect that $\mathbf{M}(t)$ constitutes a

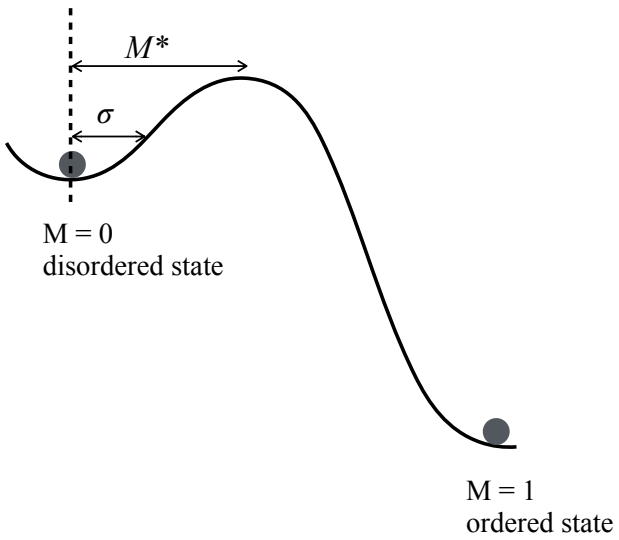

Figure 2.10: Schematic illustration of phenomenological potential landscape in the global polarization space. The disordered state is metastable; the parameter fluctuates in the potential with the amplitude σ. Stochastic crossing of the potential barrier drives the system into the absorbing ordered state.

two-dimensional Ornstein-Uhlenbeck process[67]. The stationary distribution of the radial component $M(t)$ should be given by a Rayleigh distribution,

$$f(M) = \frac{M}{\sigma_M^2} \exp\left(-\frac{M^2}{2\sigma_M^2}\right), \tag{2.6}$$

where the scale parameter σ_M is the characteristic amplitude of the fluctuation. In fact, the observed distribution can be fitted reasonably by a Rayleigh distribution (Fig. 2.11(a)), providing an estimate of σ_M as

$$\sigma_M^2 = \frac{1}{2t} \int_0^t \left(M(t')\right)^2 dt'. \tag{2.7}$$

Aside from the fluctuation amplitude, the escape rate is determined by the "position" of the barrier in order parameter space, which can be estimated by preparing a system in which a fraction of particles are given an identical polarity so that initial polarization $M(0)$ has a finite value. The initial positions are uniformly distributed both for aligned and unaligned particles. The double-well potential picture suggests that the time development of the system depends on which side of the barrier the initial state is situated: Systems with

$M(0)$ smaller than a certain value relax to the disordered state and those with $M(0)$ larger than the same threshold goes to the ordered state. The threshold M^* indicates the position of the barrier (Fig. 2.11(b)).

Decreasing γ in the disorder region towards the transition point, the threshold M^* decreases (Fig. 2.11(c)) and the fluctuation amplitude σ_M increases (Fig. 2.11(d)). These results imply that the escape rate increases and the average time until spontaneous polarization occurs will be shorter.

Due to the absence of noise, a fully-ordered system does not evolve back to a disordered state; the ordered state is an absorbing state. We also study the stability of the ordered state numerically. The initial polarities are set to be aligned except for a small fraction (5 to 20% of all particles) with random directions. The initial positions are, again, uniformly distributed both for aligned and unaligned particles. In all the realizations, the system quickly relaxes to a fully ordered state, even if we choose a parameter set deep in the disordered phase, such as $\Phi = 0.2, \gamma = 50$. This result suggests that the ordered state is stable against perturbation.

2.6 Summary

In this Chapter, we constructed a repulsive self-propelled particle model by following several principles. We emphasize that this model is consistent with some other models presented in previous studies.

- Soft particle models for epithelial cell migration developed in Refs. [58, 60] has a first order equation of motion instead of Eq. (2.1), namely $\dot{\mathbf{r}}_i = v_0\hat{\mathbf{e}}(\psi_i) + \sum_j \mathbf{f}_{ij}$, where v_0 is a constant speed. This model is equivalent to ours when we take the overdamped limit, $\beta \to \infty$ with $\alpha/\beta = \text{const}$.

- The model mentioned in Ref. [68] and explored in Ref. [62] does not have the polarity degree of freedom and employs the following equation of motion: $\dot{\mathbf{v}}_i = v_0\hat{\mathbf{v}}_i - \mathbf{v}_i + \sum_j \mathbf{f}_{ij}$, which means self-propulsion is always directed towards the direction of motion. This model corresponds to another limit in our model, $\gamma \to \infty$.

- The social force model[36] is given by the following dynamics: $\dot{\mathbf{v}}_i = v_0\hat{\mathbf{d}}_i - \mathbf{v}_i + \sum_j \mathbf{f}_{ij}$, where $\hat{\mathbf{d}}_i$ denotes the individual's desired direction. This equation of motion is analogous to $\gamma = 0$ case in our model, where the polarity of particles are never changed, although the particular form of short-range repulsive interaction differs.

Hence, our model can be regarded as a generalization that bridges the above three models. While these previous models incorporate noise as a control parameter, we show that the phase transition is realized even in the absence of noise. Close to the critical point, the dynamics of the system is characterized by a long waiting time followed by a rapid transition from the disordered state to the ordered state. By focusing on the waiting time distribution, we find the Poissonian character of the ordering process. A phenomenological picture of double-well potential that aims to explain the stochastic state transition conforms to the results from many-particle simulations. Moreover, the change in the shape of the potential landscape alters the metastability of the disordered state, inducing a phase transition.

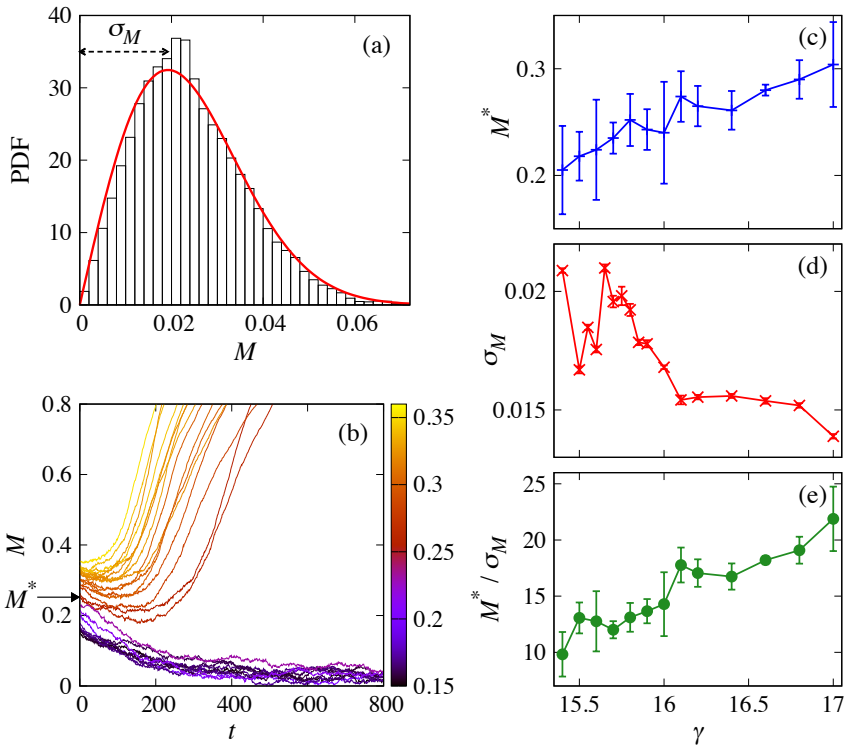

Figure 2.11: All the figures represent the data for $N = 10000, \Phi = 0.2$. (a) Normalized distribution of M in a disordered state, obtained from four independent runs with $\gamma = 15.8$ and $T = 5000$, fitted by probability density function of a Rayleigh distribution with scale parameter σ_M (red solid curve). (b) Time series of M in initially asymmetric runs with $\gamma = 15.8$. Colors correspond to the initial values $M(0)$ as indicated by the color bar. Polar order quickly emerges with $M(0) > M^*$. (c)(d) γ dependence of M^*, which decreases as γ approaches $\gamma_c \simeq 15.6$ from above, and of σ_M, which increases, respectively. (e) The ratio between the two values decreases, suggesting that the fluctuation of M is more likely to lead to an escape from the metastable, disordered state by crossing the potential barrier.

Chapter 3

Kinetic approach

3.1 Introduction

Efforts to derive a continuum theory of active matter has been initiated by Toner and Tu[24, 25], who formulated a hydrodynamic expression of macroscopic fields based on the symmetry and conservation considerations. Their theory provides an effective description for the Vicsek model, that the nonzero speed of the particles enhances the domain of alignment of interaction with other particles and thus account for the emergence and stabilization of the long-range order. They also predicted that long wavelength instability and giant number fluctuations arise from the broken rotational symmetry, which is later confirmed by numerical simulations[22].

Despite its ability to address the general features of the active matter, Toner-Tu theory is not able to calculate the transport coefficients from the microscopic parameters. It also misses clustering and segregation observed in the simulations of Vicsek model, mainly because the treatment of noise term is elusive. To overcome these shortcomings, one has to resort to a coarse-graining method. Such approach was developed by Bertin et al.[69, 70], who constructed a kinetic theory starting from the Boltzmann equation. Later, the expansions of this approach up to higher order has been made using the Boltzmann-Ginzburg-Landau framework[71, 72, 73] and the Enskog-type approach[74]. Here, I will briefly depict the outline of this Boltzmann formalism.

The main idea is to obtain a mesoscopic description of the evolution of the system by one-particle distribution $f(\zeta)$ in the phase space, where ζ denotes the set of relevant variables, from the microscopic dynamics. The hydrodynamic equations should be derived by integrating this mesoscopic equation. Let us consider a dilute limit where only binary interactions take place. The Vicsek model assumes an equal constant speed for all the particles, so $\zeta = (\mathbf{r}, \theta, t)$,

where θ is the heading direction of the velocity. The speed is a time-dependent variable for the repulsive SPP model, but as we deal with a dilute system, it quickly relaxes to the stationary one compared to the time scale where a particle runs the mean free path. In other words, particles are always fully relaxed before every collision in terms of the velocity and the polarity. Hence, we can think that $\zeta = (\mathbf{r}, \theta, t)$ in this case too.

The Boltzmann equation is written as

$$\frac{\partial f(\mathbf{r},\theta,t)}{\partial t} + v\hat{\mathbf{e}}(\theta)\cdot\nabla f(\mathbf{r},\theta,t) = I_{\mathrm{dif}}[f] + I_{\mathrm{col}}[f^{(2)}]. \tag{3.1}$$

The second term of the left hand side stems from the streaming equation, that is, Eq. (1.5) for the Vicsek model and Eq. (2.1) in the repulsive SPP model, with stationary speed v and unit vector $\hat{\mathbf{e}}(\theta)$ in the direction of motion. I_{dif} accounts for self-diffusion caused by angular fluctuation; this term does not exist in the repulsive SPP model due to the deterministic character. Finally, I_{col} describes the contribution of binary collisions. It generally depends on the two-particle distribution $f^{(2)}(\mathbf{r}, \theta_i, \theta_j, t)$. Here, we employ the "molecular chaos" assumption, which approximates the two-particle distribution as the product of one-particle distributions,

$$f^{(2)}(\mathbf{r},\theta_i,\theta_j,t) \simeq f(\mathbf{r},\theta_i,t) f(\mathbf{r},\theta_j,t). \tag{3.2}$$

This assumption signifies that the collisions are not correlated to each other.

The collision integral I_{col} is given by the sum of a loss term $(-)$ and a gain term $(+)$,

$$I_{\mathrm{col}}^{-} = -f(\mathbf{r},\theta,t)\int_{-\pi}^{\pi} \mathrm{d}\theta'\, \Gamma(\theta',\theta) f(\mathbf{r},\theta',t), \tag{3.3}$$

$$I_{\mathrm{col}}^{+} = \int_{-\pi}^{\pi}\mathrm{d}\theta_1 \int_{-\pi}^{\pi}\mathrm{d}\theta_2\, \Gamma(\theta_1,\theta_2) f(\mathbf{r},\theta_1,t) f(\mathbf{r},\theta_2,t) \times \int_{-\infty}^{\infty}\mathrm{d}\eta\, P(\eta)\, \delta_{2m\pi}(\Psi(\theta_1|\theta_2) + \eta - \theta), \tag{3.4}$$

where $\delta_{m\pi}$ is a generalized Dirac delta function imposing that the argument is equal to zero modulo $m\pi$, or explicitly defined as $\delta_{2m\pi}(\theta) = \sum_{m=-\infty}^{\infty}\delta(\theta + 2m\pi)$.

The collision kernel $\Gamma(\theta_1, \theta_2)$ is the so-called differential scattering cross section, collision rate for particles moving in θ_1 and θ_2. Both for the Vicsek

model and the repulsive SPP model, it is given as

$$\Gamma(\theta_i, \theta_j) = 2va\,|\hat{\mathbf{e}}(\theta_i) - \hat{\mathbf{e}}(\theta_j)| = 4va\left|\sin\frac{\theta_{ij}}{2}\right|, \tag{3.5}$$

where a is the interaction range and θ_{ij} is the relative angle between θ_i and θ_j. η denotes the angular noise drawn from the distribution $P(\eta)$; again, we can set $\eta = 0$ and ignore the integral with respect to η for the deterministic case.

Given that particle i and j collide with pre-collisional directions θ_i and θ_j, respectively, the function$\Psi(\theta_i|\theta_j)$ returns the post-collisional direction of particle i. For the Vicsek model, it has a simple form,

$$\Psi(\theta_i|\theta_j) = \frac{1}{2}(\theta_i + \theta_j). \tag{3.6}$$

However, for the repulsive SPP case, more calculation is necessary to obtain $\Psi(\theta_i|\theta_j)$, as we will see in the next sections.

Once we have the Boltzmann equation, we can obtain hydrodynamic equations by Fourier expansion of one-particle density f with respect to the angular variable θ and calculate all transport coefficients; I will not go into detail here, but interested readers can look for the procedure in references[69, 70, 72, 61, 73].

The uniform distribution is the trivial solution of the Boltzmann equation. One can test the stability of the isotropic state against the fluctuaions: to this end, Lam et al.[75] proposed the von Mises distribution ansatz, which links the global order parameter and the one-particle angular distribution. By linearizing the distribution, they explained the nature of the instability of isotropic state.

In this chapter, we give a much more simple understanding on the mechanism that underlies the ordering behavior shown in the previous section by focusing on the binary particle collision process. We numerically derive Ψ, or the input-output mapping of collision. We try to expand the method for application in the finite density regime.

3.2 Binary scattering analysis in dilute limit

In this section, we assume that the system is dilute ($\Phi \to 0$) so that the collisions are uncorrelated with each other, and that both the velocity and the polarity are fully relaxed before every collision.

Let us consider a binary scattering process between particle i and j (Fig. 3.1).

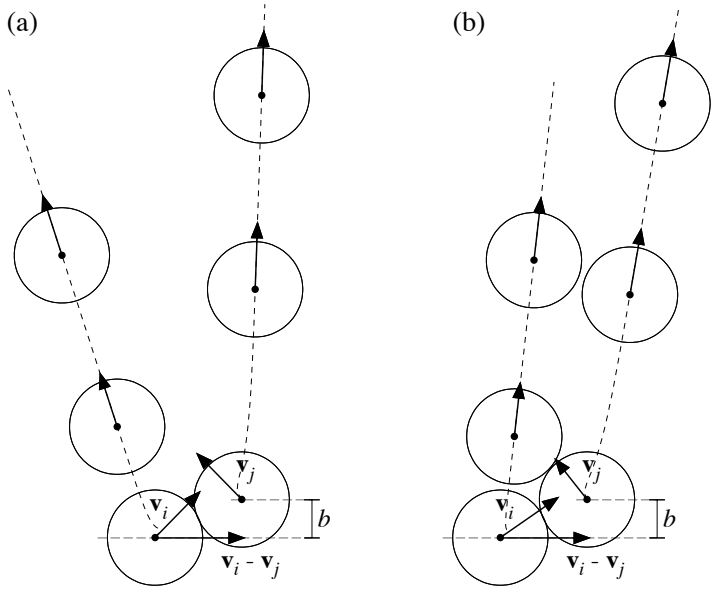

Figure 3.1: Illustration of binary scattering. (a) In dilute limit, the velocity of the two particles are fully relaxed ($v_i = v_j = \alpha$) before collision. The geometry of binary collision is fully specified by the relative angle $\theta_{ij} = \arccos(\mathbf{v}_i \cdot \mathbf{v}_j / v_i v_j)$ of the velocities and impact parameter b. (b) For finite densities, the velocities may not be at the stationary speed at the moment of contact. Here, the relative velocity $\mathbf{v}_i - \mathbf{v}_j$ and the impact parameter b are equal to those in (a), but the velocities are set to be $v_i = 1.1\alpha, v_j = 0.8\alpha$. The consequent trajectory differs from the dilute case.

Since we assume the rotational invariance, the geometry of the moment of contact is fully specified by two scalar parameters: the impact parameter

$$b = \sqrt{r_{ij}^2 - \mathbf{r}_{ij} \cdot (\mathbf{v}_i - \mathbf{v}_j)/v_{ij}} \in [0, a), \tag{3.7}$$

where $v_{ij} = |\mathbf{v}_i - \mathbf{v}_j|$, and the relative angle

$$\theta_{ij} = |\theta_i - \theta_j| \in (0, \pi]. \tag{3.8}$$

The impact parameter shows the perpendicular offset of the two bodies' center of mass from head on collision. If $b = 0$ the collision is head on whereas it is a miss if $b > a$.

Instantaneous alignment of the two particles is characterized by two-particle

polarization,

$$M^{(2)} = \frac{1}{2} \left| \hat{\mathbf{e}}(\theta_i) + \hat{\mathbf{e}}(\theta_j) \right| , \tag{3.9}$$

which corresponds to Eq. (2.4) with $N = 2$. We measure the post-collisional two-particle polarization $M^{(2)}_{\rm out}$ at the point where the polarities and the velocities are fully relaxed, and compare it to the pre-collisional polarization $M^{(2)}_{\rm in}$. The increment $\Delta M^{(2)} = M^{(2)}_{\rm out} - M^{(2)}_{\rm in}$ indicates the magnitude of parallel alignment caused by the scattering process.

Assuming the system is homogenous and isotropic, two particles should collide in the relative angle of θ_{ij} with a probability proportional to the relative velocity v_{ij}; the impact parameter b should be uniformly distributed. The average tendency of binary alignment, as a function of γ, is then obtained by taking an integral weighted by the "scattering cross section,"

$$\langle \Delta M^{(2)} \rangle = \frac{1}{C} \int_0^{\pi} \int_0^{2a} \left| \sin\left(\frac{\theta_{ij}}{2} \right) \right| \, \Delta M^{(2)}(\theta_{ij}, b) \, \mathrm{d}b \, \mathrm{d}\theta_{ij}, \tag{3.10}$$

where C is a normalization constant.

Fig. 3.2 shows $\Delta M^{(2)}$ as a function of the magnitude of relative velocity $v_{ij} = \sqrt{2 - 2\cos\theta_{ij}}$ and the impact parameter b.

The result shown in Fig. 3.3 indicates that the alignment tendency has a maximum at $\gamma \sim 1$. For $\gamma \to 0$, which corresponds to the regime where angular relaxation is slow, $\langle \Delta M^{(2)} \rangle$ goes to zero. For large γ, namely $\gamma \to \infty$, $\langle \Delta M^{(2)} \rangle$ has a negative value.

Qualitative explanation is as follows. If the rotational damping is weak, the polarity of two particles remain unchanged, so the directions of motion will eventually restored to the original direction. In contrast, if the damping is strong, the polarity rotates itself quickly to follow the change in the direction of motion. It is with an intermediate value of the damping strength that the motion of two bodies align parallel, due to the competing effect of repulsive collision and subsequent rotational damping.

This argument is consistent with the results obtained from the many-particle simulations: First, the ordering in many-body system is the fastest in the parameter region that maximizes the value of $\langle \Delta M^{(2)} \rangle$; second, the transition point in a dilute system is in agreement with the zero-crossing point (Fig. 2.7). These agreements imply that the onset of the collective motion arises from iteration of binary scattering, although one will have to take into account many-body correlation for the late stage of the ordering process, where the isotropic and uncorrelated conditions no longer hold.

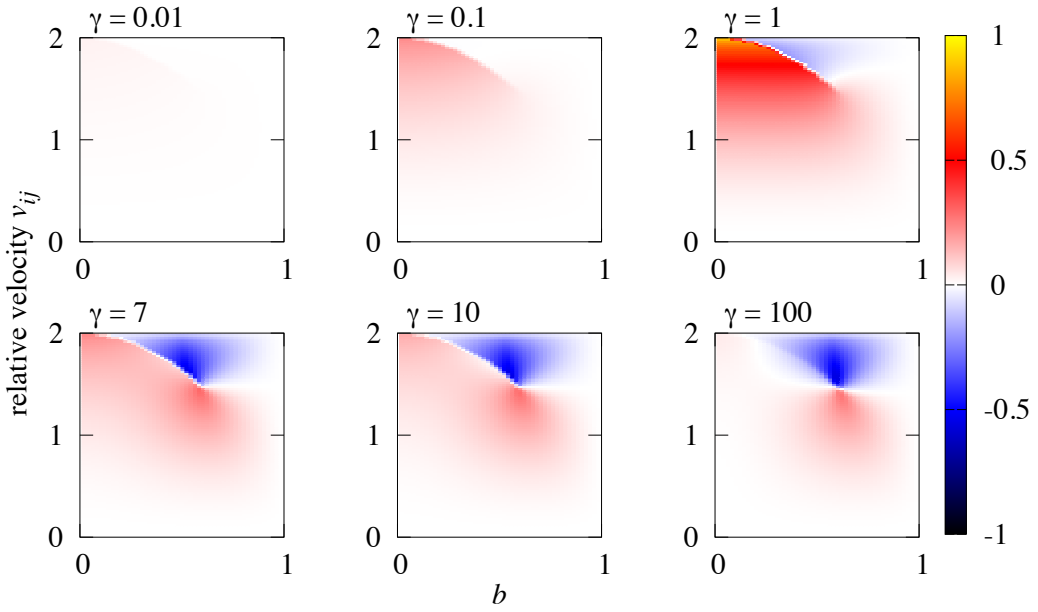

Figure 3.2: Binary alignment $\Delta M^{(2)}$ as a function of the magnitude of relative velocity $v_{ij} = \sqrt{2 - 2\cos\theta_{ij}}$ and the impact parameter b.

3.3 Expansion for finite densities

The analysis in the previous section is only valid for dilute limit, where the velocity and the polarity of the particles are fully relaxed before every collisional event. At finite densities, however, the relaxation may not complete between collisions (Fig. 3.1).

For the parameter values we choose ($\alpha = 1$ and $k = 100$), $\gamma \gg \beta = 1$ in the disordered phase, meaning that relaxation of polarity is much faster than that of velocity. We check this by measuring the speed $v_i = |\mathbf{v}_i|$ and the deviation $\theta_i - \psi_i$ between direction of velocity and polarity of all the particles directly from the many-particle simulation. Fig. 3.4 shows that the distribution of v_i is considerably broad compared to the polarity distribution, which has a narrow peak at the point where $\theta_i = \psi_i$. We will therefore take into account the speed distribution while safely neglecting the angular deviation in the following.

We apply a similar binary scattering study as in the previous section, except that $M^{(2)}_{\text{out}}$ is not defined at the point where the relaxation is complete, but at the point where the particle reaches the distance of the mean free path (mfp) away from the binary contact.

To calculate the mfp, we assume that every particle moves at speed v. The

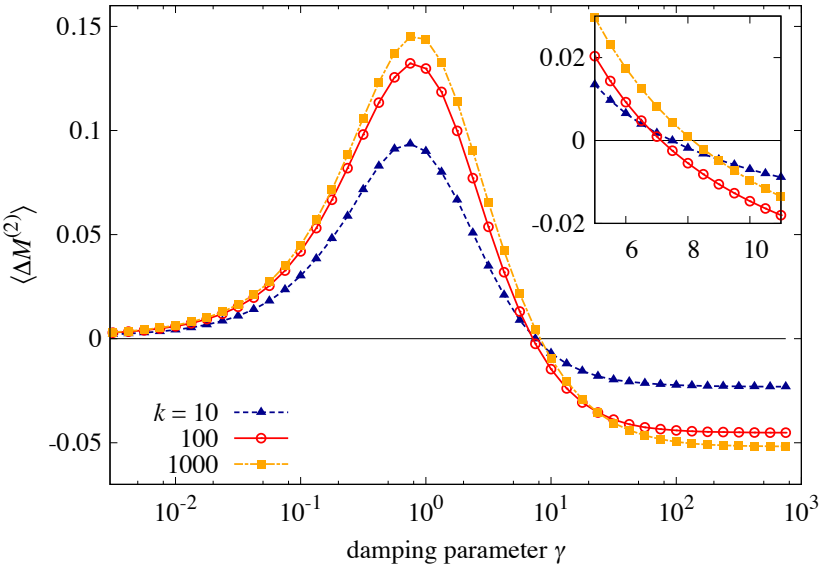

Figure 3.3: Average binary alignment $\langle \Delta M^{(2)} \rangle$ as a function of angular damping parameter γ. The tendency of alignment reaches its maximum at $\gamma \sim 1$ and decreases to take negative values for larger γ. Inset: zoom of the zero-crossing point.

magnitude of relative velocity between two particles is

$$v_r = 2v \sin\left(\frac{\theta_{ij}}{2}\right). \tag{3.11}$$

If collisions are uncorrelated to each other, the mean relative velocity is

$$\langle v_r \rangle = \frac{1}{\pi} \int_0^{\pi} 2v \sin\left(\frac{\theta_{ij}}{2}\right) \mathrm{d}\theta_{ij} = \frac{4v}{\pi}. \tag{3.12}$$

Since the scattering cross section $s = 4a$ and the number density $n = \Phi/a^2\pi$, the mfp is given as

$$\lambda = \frac{v}{sn\langle v_r \rangle} = \frac{a\pi^2}{16\Phi}. \tag{3.13}$$

Suppose particles i and j of speed v_i and v_j come into contact and are scattered. We assume that the speed of the particles independently obeys an identical distribution $f(v)$. The speeds evolve to v_i' and v_j' when the particles travels the distance of mfp after the collision. The post-collision speed

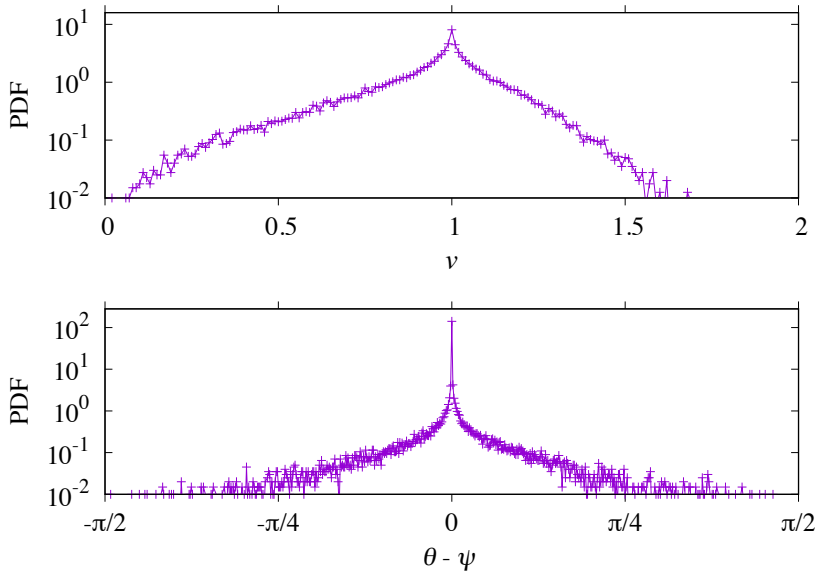

Figure 3.4: Instantaneous distribution of speed (top) and of angular deviation between velocity and polarity (bottom) in a run with parameter values in the disordered phase ($\Phi = 0.2, \gamma = 18, t = 5000$). The speed is distributed broadly, while the angle distribution has a much narrower peak at 0, suggesting most of the particles are relaxed in terms of rotational degree of freedom.

distribution can be written as

$$f(v') = \hat{S} f(v), \tag{3.14}$$

where $\hat{S}$ denotes the scattering operator.

If the system is in the disordered phase, then the distribution is stationary, so the following self-consistent condition should be satisfied:

$$\hat{S} f_s(v) = f_s(v), \tag{3.15}$$

where $f_s(v)$ is the stationary distribution. According to the Perron-Frobenius theorem[76], $f_s(v)$ is the eigenfunction of operator $\hat{S}$ which corresponds to the eigenvalue one.

$\hat{S}$ is numerically derived by mapping pre-collision speeds (v_i, v_j) onto post-collision speeds (v_i', v_j'). We divide the v-space into bins and simulate a binary scattering process for the representative value for each bin to obtain the matrix $\hat{S}$. Applying the power iteration method, we yield $f_s(v)$ as the eigenvector of $\hat{S}$.

Once $f_s(v)$ is known, the averaged increment in the two particle polarization is calculated as

$$\langle \Delta M^{(2)} \rangle = \frac{1}{C} \int_0^\infty \mathrm{d}v \int_{v_i - v_j}^{v_i + v_j} \mathrm{d}v_{ij} \int_{-a}^{a} \mathrm{d}b \, \frac{f_s(v)}{v_{ij}} \Delta M^{(2)}(v_i, v_j, v_{ij}, b), \tag{3.16}$$

where $v_{12} = |\mathbf{v}_1 - \mathbf{v}_2|$ and C is a normalization constant.

Again, by numerically calculating the point where $\langle \Delta M^{(2)} \rangle$ crosses zero, we obtain the estimated phase boundary. However, the estimation deviates from the results of many-body simulations, as shown in Fig. 2.7. The binary scattering approach is based on three assumptions: (i) the collisions are uncorrelated to each other; (ii) the motion of the particles is isotropic; (iii) the system is homogeneous, i.e., the density does not fluctuate. We suppose that these assumptions basically contribute to suppress the emergence of ordering behavior and that the deviation with the results from many-body simulations stems from the failure of one or more of the assumptions. A more detailed analysis of this point, particularly a closer look into the local quantities, is left for future work.

3.4 Summary

The kinetic approach to the dynamics of repulsive SPP uncovered that the physics that induces the emergence of the collective motion is the iteration of binary collision and the rotational relaxation afterwards. This argument is supported by the fact that the binary scattering analysis predicts the transition point from the many-particle simulation in the dilute limit. For finite densities, however, the approach deviates from the actual boundary because the disordered state is unstable against the many-particle correlations, anisotropy of the collisions, and the density fluctuation in the system.

Chapter 4

Effects of geometry and boundaries

4.1 Introduction

In the last two Chapters, we explored the characteristics of systems under the periodic boundary conditions. Periodic boundaries gain a long-standing popularity in the history of computational statistical physics, especially in the context of molecular dynamics simulation, because it is useful for approximating the bulk properties of many equilibrium systems. However, it has some limitations: an artificial order may be imposed because of the periodicity that can lead to abnormal results for structural and dynamical properties obtained from the simulation. In equilibrium systems, finite size analysis is a convenient way to infer the asymptotic behavior in the thermodynamic limit. However, the method may neither be justifiable nor come in handy when applied to systems strongly out of equilibrium. Therefore, the effects of geometry and boundaries should be tested and compared with the results with periodic boundary conditions.

Another reason we should consider various geometries and boundary conditions is that it is easier to draw an analogy to the physical systems. In the embryonic development process, the collective cell migration involves all stages of morphogenesis of multicellular structures. Usually this kind of migration occurs under a certain spatial confinement. For example, the epithelial surface of spherical *Drosophila* egg chamber exhibits a coordinated rotational motion within the space sandwiched between follicle cells and the extracellular matrix (ECM) during the elongation of the organism[77]; primordial cells migrate in a quasi-one-dimensional space surrounded by ECM in the process of the development of the zebrafish lateral line[78]. Turning to the pedestrian dynamics,

people's decisions on direction of motion are often affected by the geometry of the space defined by the surrounding walls. The geometries of particular interest include straight corridors, curves, bottleneck structures, rooms with a exit, and intersections. Obstacles such as pillars, trees, and shelves also have influence on the people's behavior.

In this Chapter, we analyze the dynamics of the self-propelled particles in systems with three basic geometries: a "pipe" or "corridor" has periodic boundaries in the x direction while bounded by two reflecting walls in the y direction; a "box" or "room" is a rectangular area enclosed by walls that surround all four sides; a "disk" is a circular surface also confined by reflecting boundaries.

4.2 "Pipe" condition

First, we discuss the behavior of the system in the "pipe" condition. The vertical boundaries, perpendicular to the x axis, is periodic, while the horizontal ones, perpendicular to the y axis, is assumed to be elastic walls. The force acting on particle i in contact with the wall W is analogous with the inter-particle interaction:

$$\mathbf{f}_{iW} = -k\left(a - r_{iW}\right)\hat{\mathbf{n}}_W, \tag{4.1}$$

where r_{iW} denotes the distance to the wall W, and $\hat{\mathbf{n}}_W$ is the unit vector in the normal direction to it. The elastic coefficient k is same as that of the inter-particle interaction. Incorporating this term changes the equation of motion (Eq. 2.1) as follows:

$$\frac{\mathrm{d}\mathbf{v}_i}{\mathrm{d}t} = \alpha\hat{\mathbf{e}}(\psi_i) - \beta\mathbf{v}_i + \sum_j \mathbf{f}_{ij} + \sum_W \mathbf{f}_{iW}. \tag{4.2}$$

We carry out the numerical simulations by employing same parameters and implementation methods as in the full-periodic case. Typical snapshots are shown in Fig. 4.1. The most significant difference from the periodic case is the segregation: the particles tend to aggregate along the elastic walls moving into either of two horizontal directions. The streams can either be in the same or in the opposite directions on the upper wall and the bottom, or it can be only along one of two sides. The direction of motion and the number of particles in the aggregates seem to have no dependence to the parameters.

We depict the phase diagram of the system as a function of volume fraction Φ and rotational damping parameter γ, as in the previous Chapter. We employ

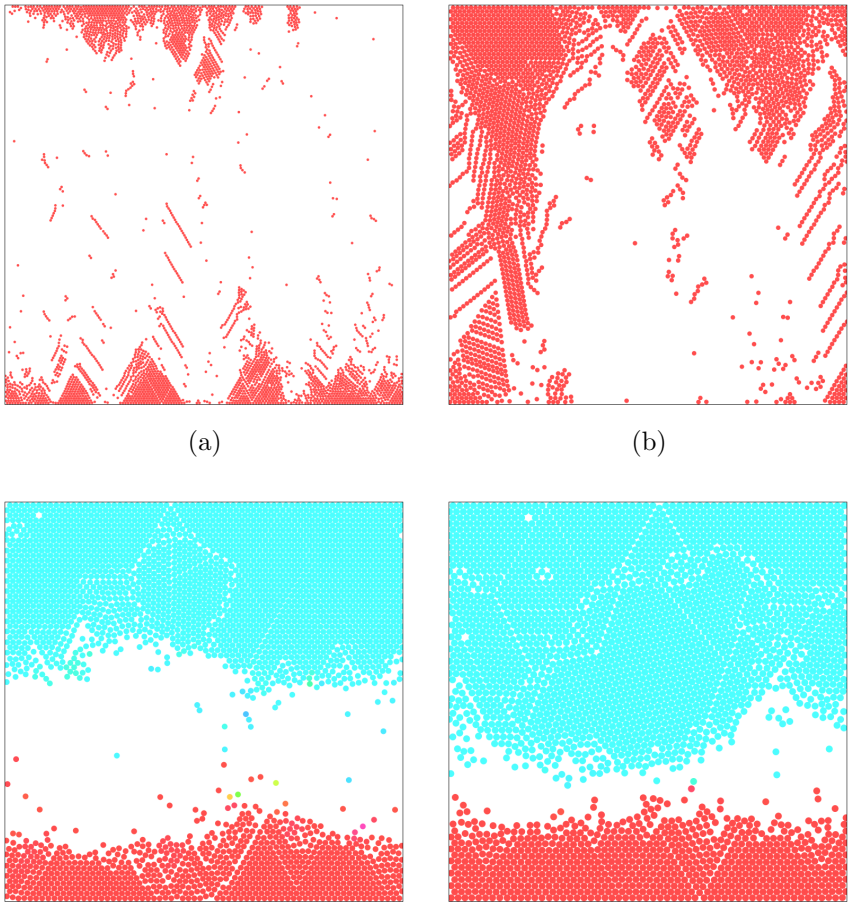

Figure 4.1: Patterns under "pipe" conditions. Parameters are $N = 3000, \gamma = 1, t = 5000$ for all figures. (a) $\Phi = 0.1$. (b) $\Phi = 0.3$. (c) $\Phi = 0.5$. (d) $\Phi = 0.7$.

the same method as the periodic case for categorizing the phase, which is to observe the time development of the system until $t = 5000$ and see if the system is in the state of coherent flow or in the disordered state. In order to quantitatively define the "coherent flow," we employ the definition of the order parameter following the previous studies on lane formation[79, 80]. Every particle i is labeled as moving to positive or negative directions along x axis depending on the sign of the projection of polarity vector, $\hat{\mathbf{e}}(\psi_i) \cdot \hat{\mathbf{x}}$. Then they are assigned an order parameter ϕ_i^{pipe}, which is equal to 1 if the lateral distance (along the y axis) $|y_i - y_j|$ to all particles j moving to the opposite direction is larger than the sum of the radius of the two particles, which in this case is $2a$; otherwise, ϕ_i^{pipe} is chosen to be zero. The global order parameter ϕ^{pipe} is

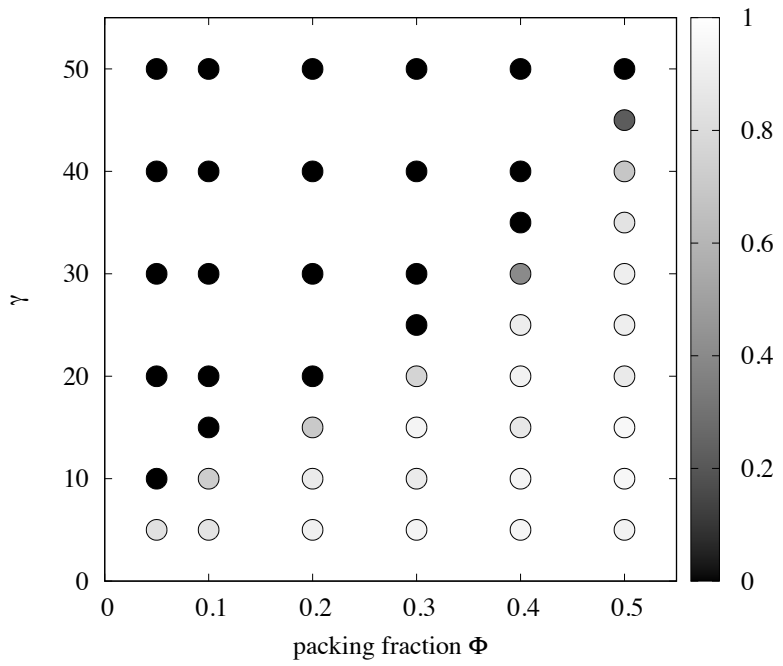

Figure 4.2: Phase diagram for $N = 5000$ systems with the "pipe" geometry. The dots are shaded black to white proportional to the time average of order parameter over 5000 time units.

defined as the fraction of "ordered" particles,

$$\phi^{\text{pipe}} = \frac{1}{N} \sum_{i=1}^{N} \phi_i^{\text{pipe}}. \tag{4.3}$$

The obtained phase diagram (Fig. 4.2) is similar to the one for the periodic case (Fig 2.7).

Fig. 4.3 shows another interesting phenomenon, observed as a transient state during some of the ordering process, where particles are dense and ordered in one part while remain disordered in the rest of the system. This coexistence of the "crystallized" region and the "gaseous" region is not a stationary state; the ordered stream eventually absorbs the particles in the gaseous region and end up in the fully ordered state where all the particles are moving into the same direction. However, the growth of order tends to be much slower and the stationary state than that in the periodic system, where the onset of growth spreads quickly to the entire system. We suppose this difference arises from the capability of propagating the particle-particle correlations. The reflecting

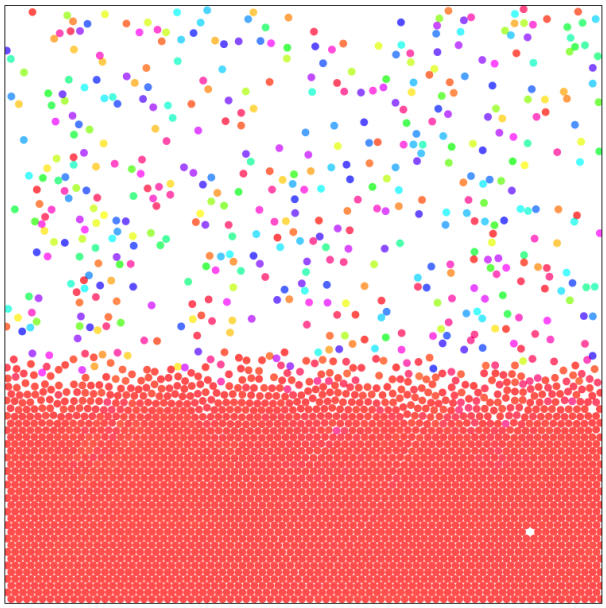

Figure 4.3: Coexistence of "gaseous" state at the top and "solid" state at the bottom. $N = 3000, \phi = 0.4, \gamma = 30, t = 4900$.

boundaries along the x axis prevent the correlations to spread from one side to another.

4.3 Confined geometries:"box" and "disk"

We now turn to the "box" condition, where all four boundaries, instead of two, consist of the reflecting walls with the same elastic property as in the "pipe" case. In contrast to the periodic and "pipe" cases, it is impossible that the entire system coherently moves into a single direction because the simulation box is enclosed and there is no inflow nor outflow of particles. The "ordered" state in this geometry is whirling motion along the boundary, as shown in Fig. 4.4.

The state with multiple vortices, whirling to the direction opposite to each other, can be regarded as a transient state under the box condition (Fig. 4.5). Once this structure is established, it persists for a considerably long time, especially for the case $\gamma \simeq 1$. This is again due to the effect of the limited correlations.

Although the transition towards coherent motion in the "box" geometry is visible when we look at the snapshots, a suitable order parameter is difficult

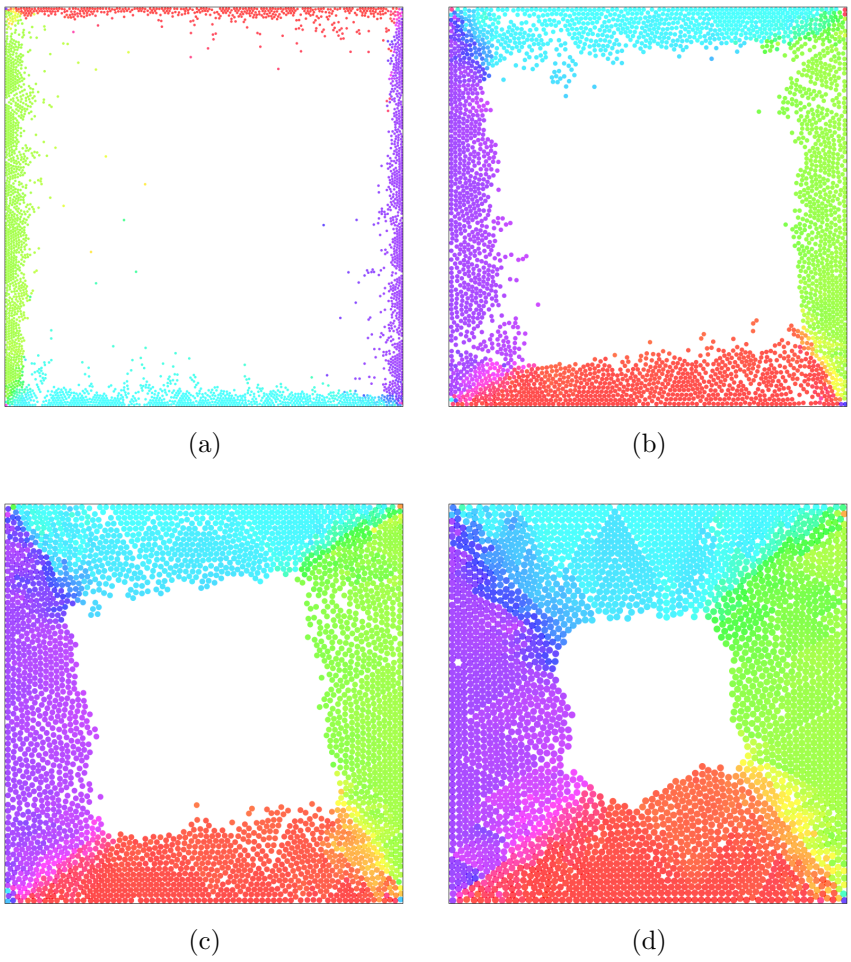

(a) (b)

(c) (d)

Figure 4.4: Patterns under "box" conditions. Parameters are $N = 3000, \gamma = 1, t = 5000$ for all figures. (a) $\Phi = 0.1$. (b) $\Phi = 0.3$. (c) $\Phi = 0.5$. (d) $\Phi = 0.7$.

to construct. Therefore, we perform simulations in another, more symmetric, confined geometry. Instead of a rectangular box, particles are placed in a simulation area enclosed by a circular reflecting wall. The packing fraction Φ is controlled by changing the radius R of the disk-shaped field as $\Phi = Na^2/R^2$. As one can expect, the coherent circular motion is observed as an ordered state under this geometrical condition as well.

The transition towards the circular flow is detected by the order parameter ϕ^{disk}, which is defined as

$$\phi^{\text{disk}} = \frac{1}{N}\left|\sum_{i=1}^{N}\frac{\mathbf{v}_i \cdot \hat{\mathbf{T}}_\omega}{|\mathbf{v}_i|}\right|, \tag{4.4}$$

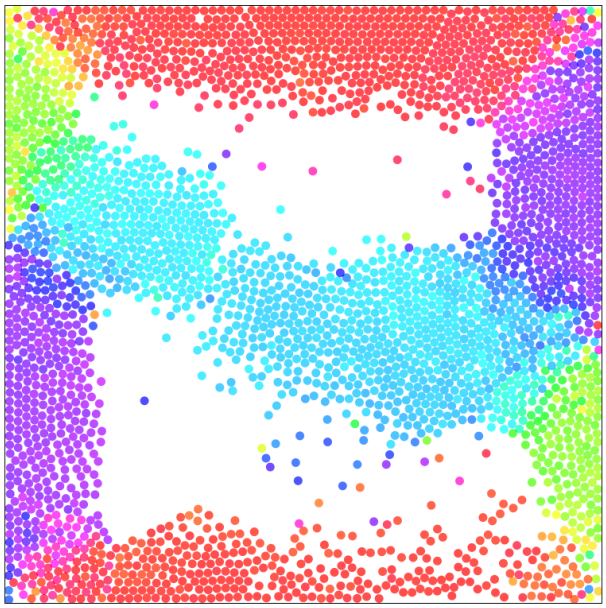

Figure 4.5: Transient state with two vortices. $N = 3000, \Phi = 0.5, \gamma = 10, t = 200$.

where ω is the angular coordinate of the particle's position in the polar coordinate system whose pole is located at the center of the disk, and $\hat{\mathbf{T}}_\omega$ denotes the unit vector in the direction of increasing ω normal to the radial direction, i.e., $\hat{\mathbf{T}}_\omega = -\sin\omega\hat{\mathbf{x}} + \cos\omega\hat{\mathbf{y}}$.

Again, we realize a number of simulations for (Φ, γ) parameter pairs and depict the phase diagram (Fig. 4.7). The fact that the phase boundary traces almost the same curve as those in the periodic and "pipe" cases leads to a conclusion that the phase transition is not affected by the boundary conditions and that the intrinsic mechanism behind the ordering behavior is indeed the microscopic correlations propagated by iteration of binary collisions.

4.4 Lane formation in bidirectional flow

Among the variety of self-organized behaviors that human crowds display, the spontaneous formation of unidirectional lanes in pedestrian counterflow is certainly one of the most popular examples that we can observe in daily urban conditions. Indeed, the phenomenon serves as one of the qualitative benchmarks to test the plausibility of a crowd simulation. Starting from random initial positions, binary mixture of pedestrians with two opposite desired di-

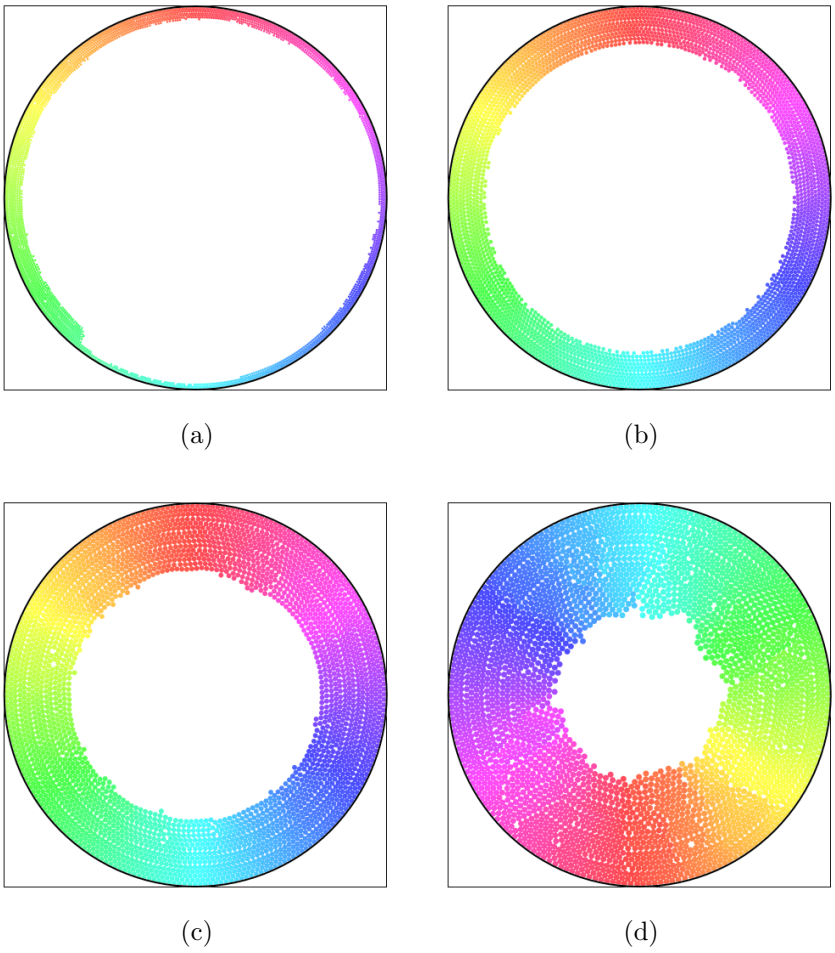

(a) (b)

(c) (d)

Figure 4.6: Patterns under "disk" conditions. Parameters are $N = 3000, \gamma = 1, t = 5000$ for all figures. (a) $\Phi = 0.1$. (b) $\Phi = 0.3$. (c) $\Phi = 0.5$. (d) $\Phi = 0.7$.

rections spontaneously separate into lanes with coherent direction of motion.

Yet, quantitative discussion on the phenomena has been scarce in the context of pedestrian dynamics by analyzing the behavior of off-lattice models. It has been rather studied in the field of colloidal dynamics: The formulation of lanes in a binary dispersion of colloidal particles, oppositely driven by an externally applied field are studied using molecular dynamics simulations, Brownian dynamics simulations, and experiments. Nonequilibrium phase transitions from a disorder to lane forming state as a function of field strength and amplitude of time-dependent oscillatory field are found by Dzubiella et al.[79]. Helbing et al.[81] reported a nontrivial jamming transition as a function of noise amplitude. By increasing the amplitude of fluctuations, which corresponds to

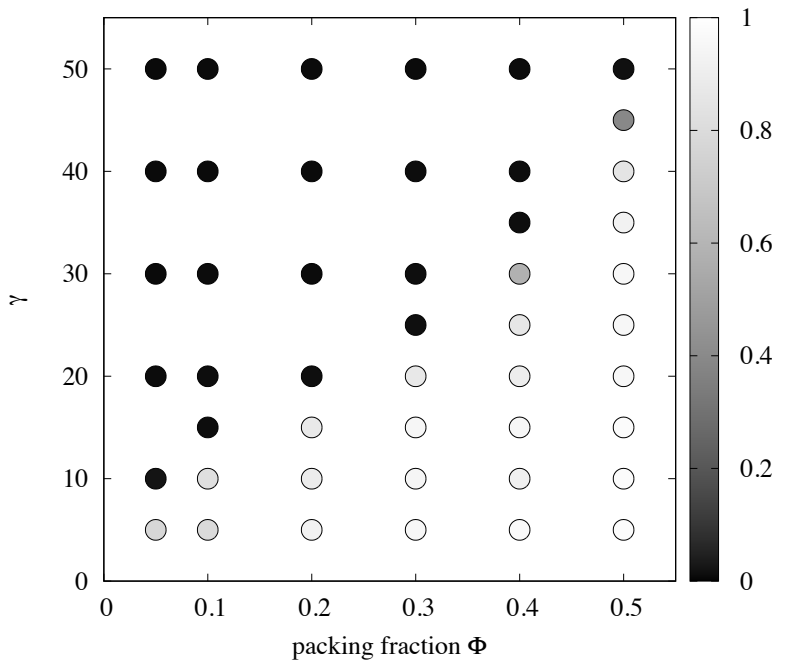

Figure 4.7: Phase diagram for $N = 5000$ systems with the "disk" geometry. The dots are shaded black to white proportional to the time average of order parameter over 5000 time units.

the temperature in thermal systems, stationary flow in lanes is hindered by the appearance of a jammed state with crystal structure. This noise-induced frozen state is destroyed by exerting additional noise, giving rise to a disordered state. Recently, oscillatory and turbulence-like behaviors are found by assuming anisotropic frictions[82].

In this section, we will first confirm the characteristics of the lane formation phenomena using the repulsive SPP model introduced in the previous Chapters. Switching off the rotation of the polarity yields a model similar to the social force model or oppositely driven particles with deterministic dynamics. Next, we will discuss the effect of inducing the rotational relaxation, which can be considered as the case where pedestrians have a finite-time memory.

We consider a simulation area with the "pipe" condition. Instead of the random initial configuration employed throughout this dissertation, we consider the case where a half of the particles have initial direction of polarity pointed toward positive direction along x-axis, $\hat{\mathbf{x}}$, and the other half to the opposite direction, $-\hat{\mathbf{x}}$. Positions are randomly distributed in the simulation area, regardless of the initial polarity.

First, we test the $d = 0$ case, where polarities are never rotated by collisions

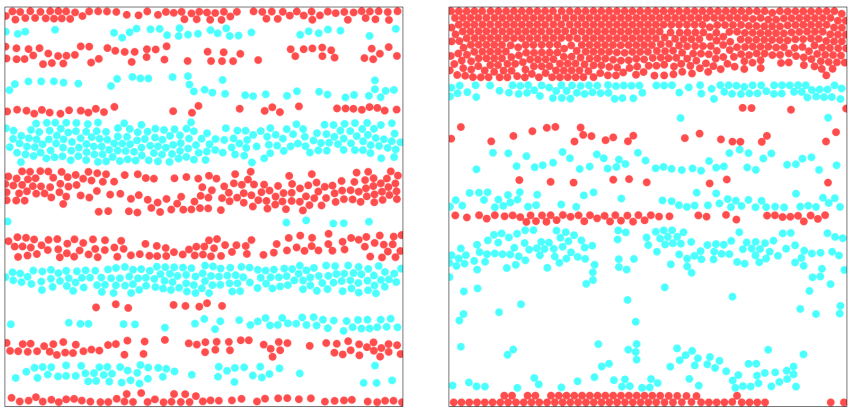

(a) (b)

Figure 4.8: Spontaneous lane formation. Introduction of weak rotational damping reduces the number of lanes. Parameters are $N = 1000, \Phi = 0.3$. (a) $\gamma = 0$. (b) $\gamma = 0.004$.

with other particles. This setting corresponds to the social force model, which assumes that each agent has their own fixed desired direction, except that the interaction is not the exponentially decaying force as usually assumed. As shown in Fig. 4.8, the spontaneous lane formation is observed. After a transitional period during which the particles collides with each other, the system reaches to a stationary state where collision and scattering no longer takes place. In this state, the binary mixture is ideally separated so that an arbitrary pair of oppositely moving particles i and j is distanced larger than the sum of their radius, $|y_i - y_j| > 2a$.

Next we apply a weak rotational damping to the particles, namely $\gamma < 0.01$. The rotational damping parameter γ indicates how fast the polarity rotates to agree the direction of motion. In other words, it expresses how fast the particle forgets its originally designated direction. From this viewpoint, we can suppose that the particles have the memory of its past polarity for limited duration of $\tau_\gamma = \gamma^{-1}$ after encounters with other particles.

The results from numerical simulations with $N = 1000$, shown in Fig. 4.9, suggest that the number of lanes are greatly reduced for increasing γ for small packing fractions. The most extreme case can be seen for $\Phi = 0.1$, where 30 lanes on average are present for $\gamma = 0$ whereas merely several lanes, in some cases a single lane in which all the particles are pointing to the same direction, is observed for $\gamma = 0.008$ and $\gamma = 0.01$. On the other hand, the number of lanes are not affected by imposing rotational damping at large densities, such

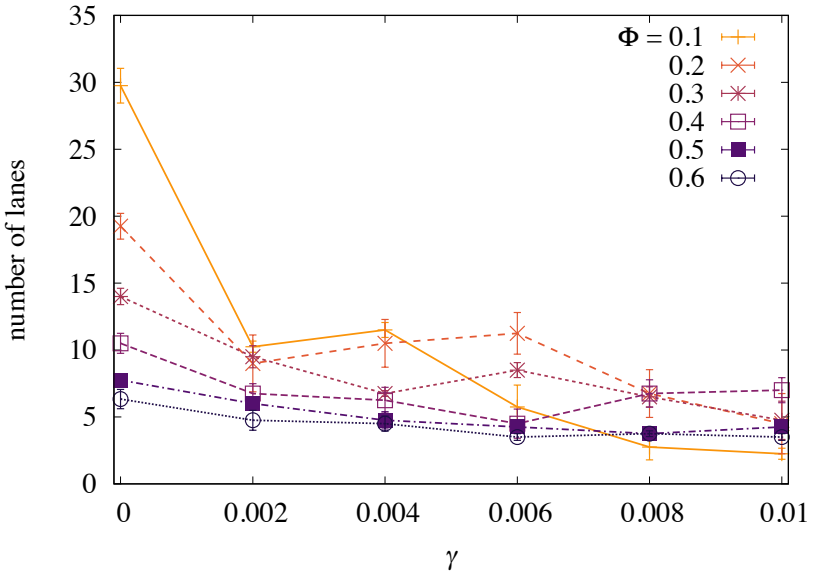

Figure 4.9: Number of lanes as a function of γ in $N = 1000$ systems.

as $\Phi = 0.5$ and $\Phi = 0.6$. Note that rotational damping is relatively weak: even for $\gamma = 0.01$, the memory of the agents last for $\tau_\gamma = 100$. Still, introducing a finite memory changes the behavior of the system, especially when the system is sparse.

4.5 Summary

In this section, we investigated the behavior of the system other than the periodic boundary condition, namely, the "pipe" and the "box" conditions. Since the microscopic mechanism leading to the coherent motion in large scales is universal in all three boundary conditions, the phase diagram is hardly changed. However, the transient states, where particles are locally aligned but the whole system have not yet reached the stationary state, tend to persist longer in the "pipe" and "box" confinements than in the periodic simulation box because the elastic walls shut off the propagation of correlation across the boundaries. We also studied the spontaneous lane formation in a binary counterflow, a phenomenon which is known well in the field of pedestrian dynamics. The rotational damping term in our model can be interpreted as how quick the agent loses the memory of its previous directions. Even with a long time memory the behavior of the system is largely altered, with fewer lanes in the stationary state.

Chapter 5

Concluding remarks

Motivated by the ubiquity of flocking behavior in biological and social systems, the physics of collective motion has been studied for decades. From the theoretical viewpoint, researches using simple mathematical self-propelled particle (SPP) models, especially the Vicsek model which assumes the ferromagnetic interaction between individuals, has contributed on the understanding on collective attributes such as ordering and clustering, that seem to be the common features among the systems composed by living organisms. On the other hand, experimental and empirical findings suggest that the interactions in real systems are much more complex and often difficult to identify. Therefore the question is to find what are the features shared beyond the Vicsek-like ferromagnetic SPP framework, and what are attributes that depend on the details of the model. To this end, we studied the collective dynamics of SPP with repulsive interactions. The repulsion is considered to be an important component in the real systems which prevents the agents from running into each other. However, few studies have addressed the nature of purely repulsive SPP systems so far; systematic understanding is still lacking.

In Chapter 2, we constructed a simple repulsive SPP model based on several principles. From numerical simulations we find the emergence of ordered motion and transition from ordered phase to disordered phase. Detailed analysis on the waiting time distribution and the dynamics of order parameter indicates that the nature of the phase transition is of first-order, that stems from the change of metastability of disordered state. When the disordered state is metastable, onset of coherent motion is induced by a nucleation process.

In Chapter 3, we studied the microscopic origin of ordering process by a binary scattering analysis. Binary collision and subsequent rotational damping of polarity, or "self-alignment" behavior, lead to an effective alignment of two particles. We attached the significance of this method to the context

of the Boltzmann approach that aims to derive the mesoscopic description of collective SPP dynamics, as well as expanding the analysis to finite density regime.

In Chapter 4, we explored the behavior of the system under geometrical constraints other than periodic boundary conditions. Looking into the ordering behavior with the "pipe," "box," and "disk" geometries, we found that the onset of local coherence is not influenced by the change in the boundary type. However, as the elastic walls place a limitation on correlation propagation across the system, transient states—the coexistence of ordered and disordered regions for "pipe" conditions and the multi-vortex structure for "box" conditions—tend to persist longer than in the system with periodic boundaries. The robustness of spontaneous lane formation behavior, one of the well-known self-organizing phenomena in the field of pedestrian dynamics, is also studied.

The repulsive SPP model into which we probed throughout this thesis is capable of accounting for many mathematical models previously proposed in wide range of field, from pedestrian movement to cell migration. Usually this kind of generalization would be associated with a complication and increase in the number of parameters in the model. To sidestep this disadvantage, the rotational damping strength is chosen to be the sole parameter to be tuned for the microscopic dynamical property. Even so, the phase transition similar to the one the Vicsek model displays is observed; this suggests that in both models, onset of order originates from the interplay of particle motion and local interaction, which explicitly or effectively contributes to the alignment. We believe our work provides an alternative perspective on the universality of collective motion.

There are some remaining topics that should point to interesting directions.

- The validity of binary scattering analysis is restricted to the dilute system, where we can assume the collisions are uncorrelated to each other. Therefore, we need another theory to describe the late stage of the order growth involving coarsening process. The first step towards this direction may be to obtain a phenomenological description on interfacial growth of ordered nucleus.

- Let us recall that an analogy has been made between the Vicsek model and classical spin systems, as we have seen in the Chapter 1. In the same sprit, comparison can be made between repulsive SPP systems and its equilibrium counterpart, which would be granular systems. Indeed, there is a increasing interest in the field on the idea that the "self-propelledness" is not limited to biological systems: vibrated granular particles

and driven colloids are also prone to exhibit collective motion. The natural question would then be as follows: how different are the physics of granular materials and that of active matter? What is the role of self-propulsion?

These problems, which are difficult to address but essential for a deeper understanding on the universality of SPP systems, are left for future work.

Bibliography

[1] Xiao-Lun Wu and Albert Libchaber. Particle diffusion in a quasi-two-dimensional bacterial bath. *Phys. Rev. Lett.*, 84:3017–3020, 2000.

[2] H P Zhang, Avraham Be'er, E-L Florin, and Harry L Swinney. Collective motion and density fluctuations in bacterial colonies. *Proc. Natl. Acad. Sci.*, 107:13626–13630, 2010.

[3] Luis Alvarez, Benjamin M Friedrich, Gerhard Gompper, and U Benjamin Kaupp. The computational sperm cell. *Trends Cell Biol.*, 24:198–207, 2014.

[4] J Elgeti, R G Winkler, and G Gompper. Physics of microswimmers—single particle motion and collective behavior: a review. *Rep. Prog. Phys.*, 78:056601, 2015.

[5] Thomas D Pollard and Gary G Borisy. Cellular motility driven by assembly and disassembly of actin filaments. *Cell*, 112:453–465, 2003.

[6] Guillaume Charras and Ewa Paluch. Blebs lead the way: how to migrate without lamellipodia. *Nat. Rev. Mol. Cell Biol.*, 9:730–736, 2008.

[7] Peter Friedl and Darren Gilmour. Collective cell migration in morphogenesis, regeneration and cancer. *Nat. Rev. Mol. Cell Biol.*, 10:445–457, 2009.

[8] Pernille Rørth. Collective cell migration. *Annu. Rev. Cell Dev. Biol.*, 25:407–429, 2009.

[9] M Poujade, E Grasland-Mongrain, A Hertzog, J Jouanneau, P Chavrier, B Ladoux, A Buguin, and P Silberzan. Collective migration of an epithelial monolayer in response to a model wound. *Proc. Natl. Acad. Sci.*, 104:15988–15993, 2007.

[10] Eric Theveneau and Roberto Mayor. Collective cell migration of epithelial and mesenchymal cells. *Cell. Mol. Life Sci.*, 70:3481–3492, 2013.

[11] Dirk Helbing, Lubos Buzna, Anders Johansson, and Torsten Werner. Self-organized pedestrian crowd dynamics: Experiments, simulations, and design solutions. *Transportation Science*, 39:1–24, 2005.

[12] Mehdi Moussaid, Dirk Helbing, Simon Garnier, Anders Johansson, Maud Combe, and Guy Theraulaz. Experimental study of the behavioural mechanisms underlying self-organization in human crowds. *Proc. R. Soc. B*, 276:2755–2762, 2009.

[13] Dirk Helbing, Anders Johansson, and Habib Al-Abideen. Dynamics of crowd disasters: An empirical study. *Phys. Rev. E*, 75:046109, 2007.

[14] Craig W Reynolds. Flocks, herds and schools: A distributed behavioral model. *ACM SIGGRAPH Computer Graphics*, 21:25–34, 1987.

[15] Ichiro Aoki. A simulation study on the schooling mechanism in fish. *Bull. Japanese Soc. Sci. Fish.*, 48:1081–1088, 1982.

[16] Akira Okubo. Dynamical aspects of animal grouping: Swarms, schools, flocks, and herds. *Adv. Biophys.*, 22:1–94, 1986.

[17] Andreas Huth and Christian Wissel. The simulation of the movement of fish schools. *J. Theor. Biol.*, 156:365–385, 1992.

[18] Iain D Couzin, Jens Krause, Richard James, Graeme D Ruxton, and Nigel R Franks. Collective memory and spatial sorting in animal groups. *J. Theor. Biol.*, 218:1–11, 2002.

[19] Yhoichi Mototake and Takashi Ikegami. A simulation study of large scale swarms. In *SWARM 2015*, pages 446–450, 2015.

[20] Tamás Vicsek, András Czirók, Eshel Ben-Jacob, Inon Cohen, and Ofer Shochet. Novel type of phase transition in a system of self-driven particles. *Phys. Rev. Lett.*, 75:1226–1229, 1995.

[21] Guillaume Grégoire and Hugues Chaté. Onset of collective and cohesive motion. *Phys. Rev. Lett.*, 92:025702, 2004.

[22] Hugues Chaté, Francesco Ginelli, and Franck Raynaud. Collective motion of self-propelled particles interacting without cohesion. *Phys. Rev. E*, 77:046113, 2008.

[23] Alexandre P Solon, Hugues Chaté, and Julien Tailleur. From phase to microphase separation in flocking models: The essential role of nonequilibrium fluctuations. *Phys. Rev. Lett.*, 114:068101, 2015.

[24] John Toner and Yuhai Tu. Long-range order in a two-dimensional dynamical xy model: How birds fly together. *Phys. Rev. Lett.*, 75:4326–4329, 1995.

[25] John Toner and Yuhai Tu. Flocks, herds, and schools: A quantitative theory of flocking. *Phys. Rev. E*, 58:4828–4858, 1998.

[26] S Ramaswamy, R Aditi Simha, and J Toner. Active nematics on a substrate: Giant number fluctuations and long-time tails. *Europhys. Lett.*, 62:196–202, 2003.

[27] Hugues Chaté, Francesco Ginelli, and Raúl Montagne. Simple model for active nematics: Quasi-long-range order and giant fluctuations. *Phys. Rev. Lett.*, 96:180602, 2006.

[28] Francesco Ginelli, Fernando Peruani, Markus Bär, and Hugues Chaté. Large-scale collective properties of self-propelled rods. *Phys. Rev. Lett.*, 104:184502, 2010.

[29] Fernando Peruani, Jörn Starruß, Vladimir Jakovljevic, Lotte Søgaard-Andersen, Andreas Deutsch, and Markus Bär. Collective Motion and Nonequilibrium Cluster Formation in Colonies of Gliding Bacteria. *Phys. Rev. Lett.*, 108:098102, 2012.

[30] Vijay Narayan, Sriram Ramaswamy, and Narayanan Menon. Long-lived giant number fluctuations in a swarming granular nematic. *Science*, 317:105, 2007.

[31] I S Aranson, A Snezhko, J S Olafsen, and J S Urbach. Comment on "long-lived giant number fluctuations in a swarming granular nematic". *Science*, 320:612, 2008.

[32] Francesco Ginelli. The physics of the vicsek model. *Eur. Phys. J. Spec. Top.*, 225:2099, 2016.

[33] L F Henderson. The statistics of crowd fluids. *Nature*, 229:381–383, 1971.

[34] Roger L Hughes. The flow of human crowds. *Annu. Rev. Fluid Mech.*, 35:169–182, 2003.

[35] Dirk Helbing and Péter Molnár. Social force model for pedestrian dynamics. *Phys. Rev. E*, 51:4282–4286, 1995.

[36] Dirk Helbing, Illés Farkas, and Tamás Vicsek. Simulating dynamical features of escape panic. *Nature*, 407:487–490, 2000.

[37] Anders Johansson, Dirk Helbing, and Pradyumn K Shukla. Specification of the social force pedestrian model by evolutionary adjustment to video tracking data. *Advs. Complex Syst.*, 10:271–288, 2007.

[38] Mohcine Chraibi, Takahiro Ezaki, Antoine Tordeux, Katsuhiro Nishinari, Andreas Schadschneider, and Armin Seyfried. Jamming transitions in force-based models for pedestrian dynamics. *Phys. Rev. E*, 92:042809, 2015.

[39] Jacques Gautrais, Francesco Ginelli, Richard Fournier, Stéphane Blanco, Marc Soria, Hugues Chaté, and Guy Theraulaz. Deciphering interactions in moving animal groups. *PLoS Comput. Biol.*, 8:e1002678, 2012.

[40] M Ballerini, N Cabibbo, R Candelier, A Cavagna, E Cisbani, I Giardina, V Lecomte, A Orlandi, G Parisi, A Procaccini, M Viale, and V Zdravkovic. Interaction ruling animal collective behavior depends on topological rather than metric distance: Evidence from a field study. *Proc. Natl. Acad. Sci.*, 105:1232–1237, 2008.

[41] Henricus H Wensink, Jörn Dunkel, Sebastian Heidenreich, Knut Drescher, Raymond E Goldstein, H. Lowen, and Julia M Yeomans. Meso-scale turbulence in living fluids. *Proc. Natl. Acad. Sci.*, 109:14308–14313, 2012.

[42] Anna Haeger, Katarina Wolf, Mirjam M Zegers, and Peter Friedl. Collective cell migration: Guidance principles and hierarchies. *Trends Cell Biol.*, 25:556–566, 2015.

[43] W J Yu, R Chen, L Y Dong, and S Q Dai. Centrifugal force model for pedestrian dynamics. *Phys. Rev. E*, 72:026112, 2005.

[44] Mohcine Chraibi, Armin Seyfried, and Andreas Schadschneider. Generalized centrifugal-force model for pedestrian dynamics. *Phys. Rev. E*, 82:046111, 2010.

[45] Ioannis Karamouzas, Brian Skinner, and Stephen J Guy. Universal power law governing pedestrian interactions. *Phys. Rev. Lett.*, 113:238701, 2014.

[46] Michele Ballerini, Nicola Cabibbo, Raphael Candelier, Andrea Cavagna, Evaristo Cisbani, Irene Giardina, Alberto Orlandi, Giorgio Parisi, Andrea Procaccini, Massimiliano Viale, and Vladimir Zdravkovic. Empirical investigation of starling flocks: a benchmark study in collective animal behaviour. *Anim. Behav.*, 76:201–215, 2008.

[47] Andrea Cavagna, Alessio Cimarelli, Irene Giardina, Giorgio Parisi, Raffaele Santagati, Fabio Stefanini, and Massimiliano Viale. Scale-free correlations in starling flocks. *Proc. Natl. Acad. Sci.*, 107:11865–11870, 2010.

[48] Yoshinori Hayakawa and Sho Furuhashi. Group-size distribution of skeins of wild geese. *Phys. Rev. E*, 86:031924, 2012.

[49] Máté Nagy, Zsuzsa Ákos, Dora Biro, and Tamás Vicsek. Hierarchical group dynamics in pigeon flocks. *Nature*, 464:890–893, 2010.

[50] B E Axelsen, L Nottestad, A Ferno, A Johannessen, and O A Misund. 'await' in the pelagic: Dynamic trade-off between reproduction and survival within a herring school splitting vertically during spawning. *Mar. Ecol. Prog. Ser.*, 205:259–269, 2000.

[51] Julia K Parrish and Leah Edelstein-Keshet. Complexity, pattern, and evolutionary trade-offs in animal aggregation. *Science*, 284:99, 1999.

[52] Steven V Viscido, Julia K Parrish, and Daniel Grünbaum. Individual behavior and emergent properties of fish schools: a comparison of observation and theory. *Mar. Ecol. Prog. Ser.*, 273:239–249, 2004.

[53] Joseph H Tien, Simon A Levin, and Daniel I Rubenstein. Dynamics of fish shoals: identifying key decision rules. *Evol. Ecol. Res.*, 6:555–565, 2004.

[54] Y Katz, K Tunstrom, C C Ioannou, C Huepe, and I D Couzin. Inferring the structure and dynamics of interactions in schooling fish. *Proc. Natl. Acad. Sci.*, 108:18720–18725, 2011.

[55] Julien Deseigne, Olivier Dauchot, and Hugues Chaté. Collective motion of vibrated polar disks. *Phys. Rev. Lett.*, 105:098001, 2010.

[56] Ivo Buttinoni, Julian Bialké, Felix Kümmel, Hartmut Löwen, Clemens Bechinger, and Thomas Speck. Dynamical clustering and phase separation in suspensions of self-propelled colloidal particles. *Phys. Rev. Lett.*, 110:238301, 2013.

[57] Daniel Strömbom. Collective motion from local attraction. *J. Theor. Biol.*, 283:145–151, 2011.

[58] B Szabó, G J Szöllösi, B Gönci, Zs Jurányi, D Selmeczi, and Tamás Vicsek. Phase transition in the collective migration of tissue cells: Experiment and model. *Phys. Rev. E*, 74:061908, 2006.

[59] D Grossman, I S Aranson, and E Ben Jacob. Emergence of agent swarm migration and vortex formation through inelastic collisions. *New J. Phys.*, 10:023036, 2008.

[60] Silke Henkes, Yaouen Fily, and M Cristina Marchetti. Active jamming: Self-propelled soft particles at high density. *Phys. Rev. E*, 84:040301, 2011.

[61] C A Weber, T Hanke, J Deseigne, S Léonard, O Dauchot, E Frey, and H Chaté. Long-range ordering of vibrated polar disks. *Phys. Rev. Lett.*, 110:208001, 2013.

[62] Timo Hanke, Christoph A Weber, and Erwin Frey. Understanding collective dynamics of soft active colloids by binary scattering. *Phys. Rev. E*, 88:052309, 2013.

[63] Julien Deseigne, Sébastien Léonard, Olivier Dauchot, and Hugues Chaté. Vibrated polar disks: spontaneous motion, binary collisions, and collective dynamics. *Soft Matter*, 8:5629, 2012.

[64] Antoine Bricard, Jean-Baptiste Caussin, Nicolas Desreumaux, Olivier Dauchot, and Denis Bartolo. Emergence of macroscopic directed motion in populations of motile colloids. *Nature*, 503:95–98, 2013.

[65] M C Marchetti, J F Joanny, S Ramaswamy, T B Liverpool, J Prost, Madan Rao, and R Aditi Simha. Hydrodynamics of soft active matter. *Rev. Mod. Phys.*, 85:1143, 2013.

[66] Yutaka Sumino, Ken H Nagai, Yuji Shitaka, Dan Tanaka, Kenichi Yoshikawa, Hugues Chaté, and Kazuhiro Oiwa. Large-scale vortex lattice emerging from collectively moving microtubules. *Nature*, 483:448–452, 2012.

[67] G E Uhlenbeck and L S Ornstein. On the theory of the brownian motion. *Phys. Rev.*, 36:823–841, 1930.

[68] Tamás Vicsek and Anna Zafeiris. Collective motion. *Phys. Rep.*, 517:71–140, 2012.

[69] Eric Bertin, Michel Droz, and Guillaume Grégoire. Boltzmann and hydrodynamic description for self-propelled particles. *Phys. Rev. E*, 74:022101, 2006.

[70] Eric Bertin, Michel Droz, and Guillaume Grégoire. Hydrodynamic equations for self-propelled particles: microscopic derivation and stability analysis. *J. Phys. A: Math. Theor.*, 42:445001, 2009.

[71] Anton Peshkov, Igor S Aranson, Eric Bertin, Hugues Chaté, and Francesco Ginelli. Nonlinear field equations for aligning self-propelled rods. *Phys. Rev. Lett.*, 109:268701, 2012.

[72] Eric Bertin, Hugues Chaté, Francesco Ginelli, Shradha Mishra, Anton Peshkov, and Sriram Ramaswamy. Mesoscopic theory for fluctuating active nematics. *New J. Phys.*, 15:085032, 2013.

[73] A Peshkov, E Bertin, F Ginelli, and H Chaté. Boltzmann-ginzburg-landau approach for continuous descriptions of generic vicsek-like models. *Eur. Phys. J. Spec. Top.*, 223:1315–1344, 2014.

[74] Thomas Ihle. Kinetic theory of flocking: Derivation of hydrodynamic equations. *Phys. Rev. E*, 83:030901, 2011.

[75] Khanh-Dang Nguyen Thu Lam, Michael Schindler, and Olivier Dauchot. Polar active liquids: a universal classification rooted in nonconservation of momentum. *J. Stat. Mech.*, 2015:P10017, 2015.

[76] Abraham Berman and Robert J Plemmons. *Nonnegative Matrices in the Mathematical Sciences*. Academic Press, 1979.

[77] Maureen Cetera, Guillermina R Ramirez-San Juan, Patrick W Oakes, Lindsay Lewellyn, Michael J Fairchild, Guy Tanentzapf, Margaret L Gardel, and Sally Horne-Badovinac. Epithelial rotation promotes the global alignment of contractile actin bundles during drosophila egg chamber elongation. *Nat. Commun.*, 5:5511, 2014.

[78] Petra Haas and Darren Gilmour. Chemokine signaling mediates self-organizing tissue migration in the zebrafish lateral line. *Dev. Cell*, 10:673–680, 2006.

[79] J Dzubiella, G P Hoffmann, and H Löwen. Lane formation in colloidal mixtures driven by an external field. *Phys. Rev. E*, 65:021402, 2002.

[80] Jerome Delhommelle. Should "lane formation" occur systematically in driven liquids and colloids? *Phys. Rev. E*, 71:016705, 2005.

[81] Dirk Helbing, Illés J. Farkas, and Tamás Vicsek. Freezing by heating in a driven mesoscopic system. *Phys. Rev. Lett.*, 84:1240–1243, 2000.

[82] Masahiro Ikeda, Hirofumi Wada, and Hisao Hayakawa. Instabilities and turbulence-like dynamics in an oppositely driven binary particle mixture. *EPL*, 99:68005, 2012.